CHALMERS
UNIVERSITY OF TECHNOLOGY

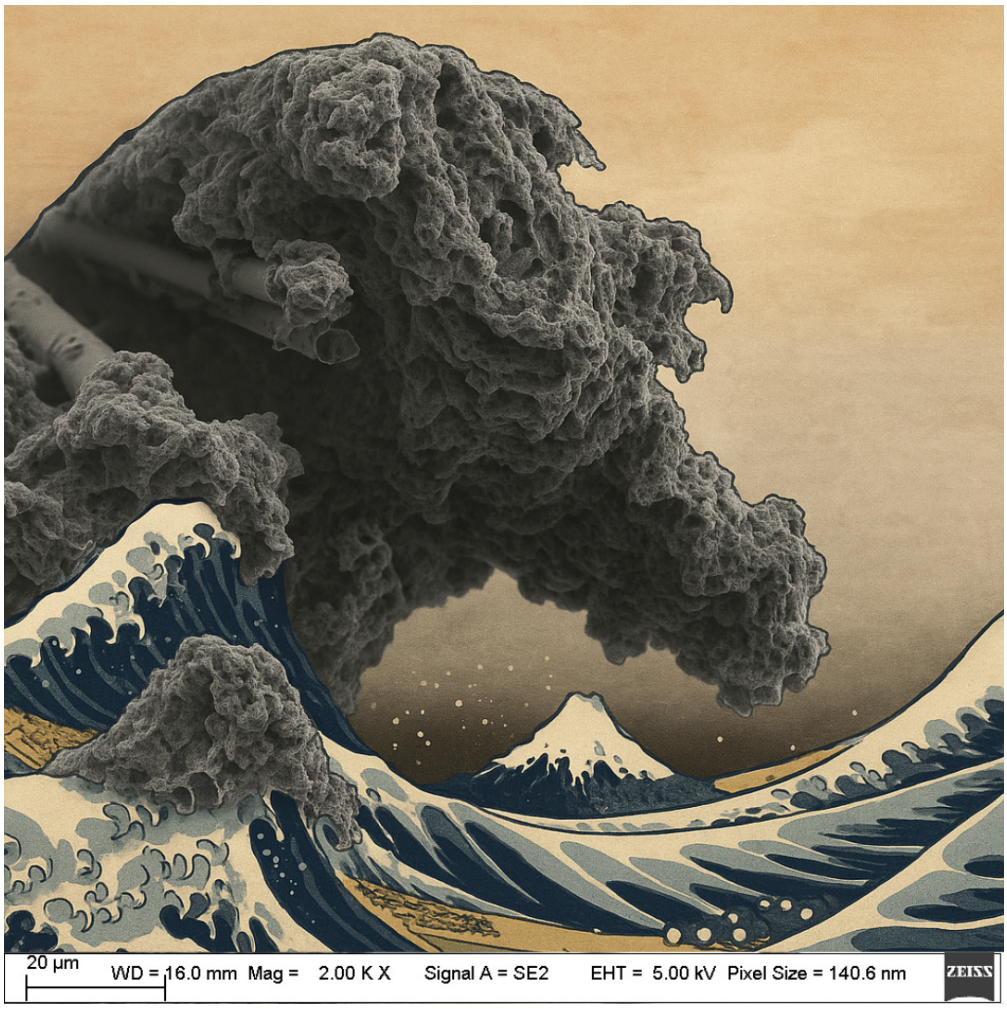

PTMA Coated Carbon Fibers

Characterization and Development Toward High Power Structural Battery Positive Electrode

Master's thesis in Applied Mechanics

SHREEYESH SREENIVASAN

DEPARTMENT OF INDUSTRIAL AND MATERIALS SCIENCE
CHALMERS UNIVERSITY OF TECHNOLOGY
Gothenburg, Sweden 2025
www.chalmers.se

Master's thesis 2025

PTMA Coated Carbon Fibers

Characterization and Development Toward High Power Structural Battery Positive Electrode

SHREEYESH SREENIVASAN

CHALMERS
UNIVERSITY OF TECHNOLOGY

Department of Industrial and Materials Science
Division of Materials and Computational Mechanics
Composites Research Group
Chalmers University of Technology
Gothenburg, Sweden 2025

PTMA Coated Carbon Fibers
Characterization and Development Toward High Power
Structural Battery Positive Electrode
SHREEYESH SREENIVASAN

Supervisor: Johanna Xu, Department of Industrial and Materials Science
Supervisor: Zhenyuan Xia, Department of Industrial and Materials Science
Supervisor: Qiaonan Chen, Department of Chemical Engineering
Examiner : Leif Asp, Department of Industrial and Materials Science

Master's Thesis 2025
Department of Industrial and Materials Science
Division of Materials and Computational Mechanics
Composites Research Group
Chalmers University of Technology
SE-412 96 Gothenburg
Telephone +46 31 772 1000

Cover: The Wave of PTMA, AI Re-imagined Scanning Electron Microscopy image of T800 Carbon fiber coated with a slurry of PTMA with reduced Graphene Oxide and Carbon Black using PVDF as the binder in N-Methyl Pyrrolidine Solvent that resembles The Great Wave of Kanagawa, by Hokusai.

Typeset in LaTeX
Printed by Chalmers Reproservice
Gothenburg, Sweden 2025

PTMA Coated Carbon Fibers:
Characterization and Development Toward High Power
Structural Battery Positive Electrode
SHREEYESH SREENIVASANN
Department of Industrial and Materials Science
Chalmers University of Technology

Abstract

Traditional batteries are often seen as structural parasites: they add weight without contributing to structural strength. Structural batteries represent a new generation of energy storage that actively reinforces structures while carrying both electrical and mechanical loads, creating multifunctional composites.

However, most multifunctional composite batteries rely on lithium-based chemistries, which are inadequate for future demands in safety, sustainability, and performance. To address these limitations, this thesis develops carbon fibers coated with poly(2,2,6,6-tetramethylpiperidinyloxy-4-yl methacrylate) (PTMA), an organic free radical polymer as a lithium-free alternative for next-generation structural batteries.

To investigate this approach, PTMA was synthesized and coated onto carbon fibers using optimized polymerization techniques. Electrochemical performance was evaluated via half-cell voltammetry and cycling testing, while microstructural analyses (SEM, FTIR, ^{1}H NMR and ^{13}C NMR) assessed coating quality and stability.

The systematic evaluation of carbon fiber electrodes with varying PTMA content (30-60 wt%) yielded promising results. Spectroscopic analysis confirmed successful PTMA synthesis and nitroxide radical formation. Cyclic voltammetry revealed that formulation F1 (30% PTMA) achieved optimal electrochemical reversibility with $\Delta E_p = 59$ mV, meeting theoretical criteria for reversible one-electron transfer. High-loading formulations demonstrated near-reversible behavior with $\Delta E_p = 119$ mV. Galvanostatic testing showed excellent capacity retention ($> 90\%$) and stable cycling performance. SEM analysis revealed successful thermal crosslinking at 175°C, transforming discrete particles into consolidated, uniform coatings with improved interfacial adhesion.

These findings demonstrate the first successful integration of PTMA with carbon fiber substrates for structural batteries. The optimized electrodes achieve reversible electrochemical behavior while maintaining mechanical integrity, establishing a foundation for sustainable, high-power structural energy storage systems and opening pathways for lightweight, multifunctional composites in aerospace and automotive applications.

Keywords: Structural Batteries, Organic Radical Batteries, Multifunctional Composites, Electrochemical Characterisation, Carbon Fibers.

Acknowledgements

I would like to express my deepest gratitude to my supervisors, Zhenyuan Xia, Johanna Xu, and Qiaonan Chen, for their unwavering guidance and invaluable expertise throughout this research journey. Their insightful feedback and hands-on help with chemical synthesis, electrochemical principles and materials science has been instrumental in shaping this work and my development as a researcher.

I extend my sincere appreciation to my examiner, Leif Asp, for his constructive criticism and valuable suggestions that significantly enhanced the quality of this research. His expertise in structural batteries and multifunctional composites provided crucial perspectives that strengthened this work.

I am grateful to the faculty and staff of the Department of Industrial and Materials Science for providing an excellent research environment and access to essential facilities. Special thanks to the laboratory technicians who assisted with SEM imaging, spectroscopic analysis, and electrochemical testing.

My appreciation extends to my fellow graduate students and colleagues for creating a collaborative and stimulating academic atmosphere. The engaging discussions about research methodologies and scientific challenges have been both educational and motivating.

On a personal note, I am profoundly grateful to my family for their unconditional love, support, and understanding throughout this academic journey. Their encouragement during challenging moments provided the emotional foundation necessary to persevere through this demanding process.

Finally, I thank my friends who provided much-needed perspective, laughter, and support outside the laboratory, helping maintain the balance essential for both personal well-being and academic success.

This work stands as a testament to the collective effort and support of all these remarkable individuals.

Shreeyesh Sreenivasan, Gothenburg, June 2025

List of Acronyms

Below is the list of acronyms that have been used throughout this thesis listed in alphabetical order:

AIBN	Azobisisobutyronitrile
CF	Carbon Fibers
CNMR	Carbon Nuclear Magnetic Resonance
CV	Cyclic Voltammetry
EC	Ethylene Carbonate
EPD	Electrophoretic Deposition
FTIR	Fourier-Transform Infrared Spectroscopy
GCPL	Galvanostatic Cycling with Potential Limitation
GMA	Glycidyl Methacrylate
GPC	Gel Permeation Chromatography
HNMR	Proton Nuclear Magnetic Resonance
IMS	Industrial and Materials Science
LFP	Lithium Iron Phosphate
$LiFePO_4$	Lithium Iron Phosphate
$LiPF_6$	Lithium Hexafluorophosphate
LiTFSI	Lithium Bistrifluoromethanesulfonylimide
mCPBA	meta-chloroperoxybenzoic acid
NMP	N-methyl-2-pyrrolidone
PC	Propylene Carbonate
PEIS	Potentiostatic Electrochemical Impedance Spectroscopy
PTMA	poly(2,2,6,6-tetramethylpiperidinyloxy-4-yl methacrylate)
PTMPM	4-methacryloyloxy-2,2,6,6-tetramethylpiperidine
PVDF	Polyvinylidene Fluoride
rGO	reduced Graphene Oxide
SEM	Scanning Electron Microscopy

Nomenclature

Below is the nomenclature of indices, sets, parameters, and variables that have been used throughout this thesis.

Indices

n	Number of electrons transferred
t	Time index

Sets

F1-F5	Set of electrode formulations
SS01-SS20	Set of sample identifications

Parameters

A	Electrode area (cm^2)
C	Bulk concentration (mol/cm^3)
D	Diffusion coefficient (cm^2/s)
F	Faraday's constant (96,485 C/mol)
I	Applied current (A)
m	Active material mass (g)
Q	Charge capacity (C)
$Q_{nominal}$	Nominal capacity
Q_{sp}	Specific capacity
R	Gas constant (8.314 J mol^{-1} K^{-1})
T	Absolute temperature (K)
v	Scan rate (V/s)

wt%	Weight percentage

Variables

E	Electrode potential (V)
E^0	Standard electrode potential (V)
$E^{0'}$	Formal potential (V)
E_{pa}	Anodic peak potential (V)
E_{pc}	Cathodic peak potential (V)
ΔE_p	Peak separation (V)
i_{pa}	Anodic peak current (A)
i_{pc}	Cathodic peak current (A)
i_p	Peak current (A)
$[Ox]$	Concentration of oxidized species (mol/cm^3)
$[Red]$	Concentration of reduced species (mol/cm^3)

Contents

List of Figures

List of Tables

1

Introduction

The integration of energy storage and structural functionality in a single material represents a significant advancement in the field of multifunctional composites. This study focuses on developing PTMA-coated carbon fibers for use in structural batteries as a positive electrode, aiming to enhance both the electrochemical performance and mechanical properties of these materials. While structural batteries utilizing carbon fiber composites have demonstrated simultaneous energy storage and load-bearing capabilities, our work introduces a critical advancement through the implementation of redox-active PTMA as an organic radical cathode. Unlike conventional lithium-ion cathodes (e.g., LFP, NMC) that rely on slow solid-state ion diffusion, PTMA's rapid nitroxide radical redox reactions are capable of exceptional power densities. This paradigm shift in charge transfer kinetics allows structural batteries to meet high-power demands in aerospace and electric vehicle applications while maintaining mechanical functionality, a dream combination unattainable with traditional intercalation cathodes.

1.1 Background

Structural batteries are multifunctional composites that store electrical energy while bearing mechanical loads. They use carbon fibers as negative electrodes and structural components, combined with a polymer electrolyte matrix that facilities ion transport and efficiently transfers structural loads. This integration allows structures to act as energy storage media, offering significant advantages in weight-critical applications like vehicle chassis and consumer electronics. Traditionally, lithium iron phosphate ($LiFePO_4$, LFP) has been the primary cathode material in structural batteries. However, LFP's limitations such as its lower energy density, relatively heavier weight, bulkier dimensions, and poorer electrical conductivity have led to exploring alternatives. One promising alternative is organic based conductive electrode materials instead of inorganic ones. For example, PTMA (poly(2,2,6,6-tetramethylpiperidinyloxy-4-yl methacrylate)), a polymer-based cathode material, is known for its stable nitroxide radicals that enable rapid charge/discharge cycles in lithium-ion batteries. However, the development of PTMA-coated carbon fibres for structural batteries involves challenges such as particle agglomeration, coating thickness control, and conductivity issues. There needs work to be done on reliable methods for coating carbon fibres with PTMA using drop casting or electrophoretic deposition (EPD) techniques (whichever is suitable for maximum coating efficiency). This approach aims to improve the performance of structural batteries, addressing

the limitations of traditional cathode materials.

1.2 Aim

The overarching goal of this Master's thesis is to explore the development of PTMA-coated carbon fibres as positive cathodes for structural battery applications. This work will focus on synthesizing the PTMA polymer and integrating it onto carbon fiber substrates through optimized coating techniques. By addressing key challenges such as achieving uniform coatings and ensuring good electrical properties, the project aims to create functional electrode materials. The electrochemical behavior of these PTMA-coated fibers will be systematically evaluated, alongside a thorough investigation of their microstructure using advanced characterization methods. Ultimately, this research aspires to contribute new insights into the design and performance of high-power multifunctional materials that combine structural integrity with energy storage capabilities.

1.3 Limitations

This work, while comprehensive, is subject to certain limitations. The focus on PTMA-coated carbon fibres may not fully represent the behavior of other potential electrode materials for structural batteries. The laboratory-scale synthesis and coating processes may not accurately reflect industrial-scale production challenges. Environmental factors such as temperature and humidity, which could affect battery performance in real-world applications, are controlled in our experimental setup and may not capture all operational scenarios. Additionally, the long-term aging effects on the PTMA coating and its interaction with the carbon fibre substrate over extended periods (beyond our cycling tests) remain uncertain. These limitations should be considered when interpreting the results and extrapolating to broader applications in structural battery development.

2

Literature Review

The development of structural batteries or multifunctional composites capable of simultaneously bearing mechanical loads and storing electrical energy, has garnered significant attention due to their potential to revolutionize lightweight, energy-storing components for transportation and aerospace applications. A critical area of innovation within this field is the integration of organic electrode materials, particularly poly(2,2,6,6-tetramethylpiperidine-1-oxyl methacrylate) (PTMA), onto carbon fibers to enhance both electrochemical performance and mechanical integration.

2.1 Structural Batteries: Concept and Recent Advances

Recent research on structural batteries has focused on combining high energy density with robust mechanical properties. State-of-the-art systems, such as those developed by Asp et al. [1], demonstrate composites achieving energy densities up to 24 Wh kg^{-1}, elastic moduli of 25 GPa, and tensile strengths exceeding 300 MPa. These results are achieved through the use of multifunctional carbon fibers, structural electrolytes, and lithium-iron-phosphate cathodes, highlighting the feasibility of structural batteries for practical applications.

Further advancements include multicell laminate architectures, which maintain electrochemical performance under mechanical loading and enable higher voltage outputs, as shown by Xu et al. [2]. Sustainable fabrication methods have also emerged, such as the use of electrophoretic deposition (EPD) with graphene additives in ethanol, which provides a greener alternative to conventional solvent-based processes and delivers high specific capacity and cycling stability [3]. Additionally, the integration of reduced graphene oxide and $LiFePO_4$ onto carbon fibers has resulted in electrodes with both high specific capacity and superior mechanical modulus, underscoring the promise of multifunctional electrode designs [4, 5].

2.2 PTMA: Synthesis, Properties, and Application in Batteries

PTMA stands out among organic cathode materials due to its high redox potential, rapid charge transfer, and cycling stability. As a p-type redox polymer, PTMA

undergoes fast and reversible electron transfer, making it suitable for high-power applications. However, the redox process involves anion transport, which introduces unique challenges in electrode design, particularly regarding electrolyte selection and electrode porosity. High mass loading PTMA electrodes can achieve areal capacities exceeding 1 mAh cm^{-2}, but require careful optimization of porosity and electrolyte content to ensure full utilization of active material and stable cycling performance.

To address PTMA's inherent solubility and adhesion issues, strategies such as thermal crosslinking have been employed. For example, PTMA-based slurries can be crosslinked on structural current collectors composed of reduced graphene oxide and aramid nanofibers, resulting in electrodes that resist delamination and maintain mechanical integrity during cycling [9]. These approaches have enabled PTMA-based structural electrodes to exhibit high rate capabilities (up to 25C), excellent specific power, and a specific modulus superior to many commercial systems. Furthermore, PTMA's compatibility with aqueous and non-aqueous systems, and its affinity for carbon-based additives, support its versatility as a cathode material [7].

Despite these advances, PTMA-based batteries still face challenges in upscaling, cost, and practical energy density compared to inorganic cathodes. The need for highly concentrated electrolytes, driven by the anion-dependent redox mechanism, increases both cost and weight, while the lower density of PTMA limits volumetric energy density. Nonetheless, the environmental benefits and rapid kinetics of PTMA continue to drive research into its integration within structural battery designs [8, 10].

2.3 Addressing the Research Gap

While the electrochemical performance and synthesis of PTMA are well documented, a significant gap remains in understanding the mechanical integration of PTMA-based electrodes within load-bearing composites. A critical gap exists in the literature regarding the integration of PTMA with carbon fibers for structural battery applications. Most existing studies focus either on the electrochemical optimization of PTMA or on the mechanical properties of structural batteries using conventional inorganic materials. There is a lack of comprehensive research addressing the interface, long-term stability, and multifunctional optimization of PTMA-coated carbon fibers in structural battery configurations. Specifically, systematic studies are needed to evaluate how PTMA adhesion, crosslinking strategies, and composite architecture impact both the mechanical and electrochemical performance over prolonged use.

Bridging this gap is crucial for the realization of lightweight, multifunctional components that can meet the demanding requirements of next-generation transportation and aerospace systems. Future research must therefore focus on the co-optimization of PTMA electrode chemistry and mechanical integration, enabling the deployment of organic radical batteries as viable alternatives to traditional metal-based systems in structural battery applications.

3

Theory

3.1 Fundamentals of Structural Batteries

A structural battery is a composite material that simultaneously performs two distinct functions: storing electrical energy and bearing mechanical loads. Unlike conventional battery systems where the battery is a separate component that adds weight to a structure, a structural battery becomes an integral part of the structure itself. The battery material literally replaces structural elements like panels, beams, or chassis components while maintaining the ability to store and deliver electrical energy.

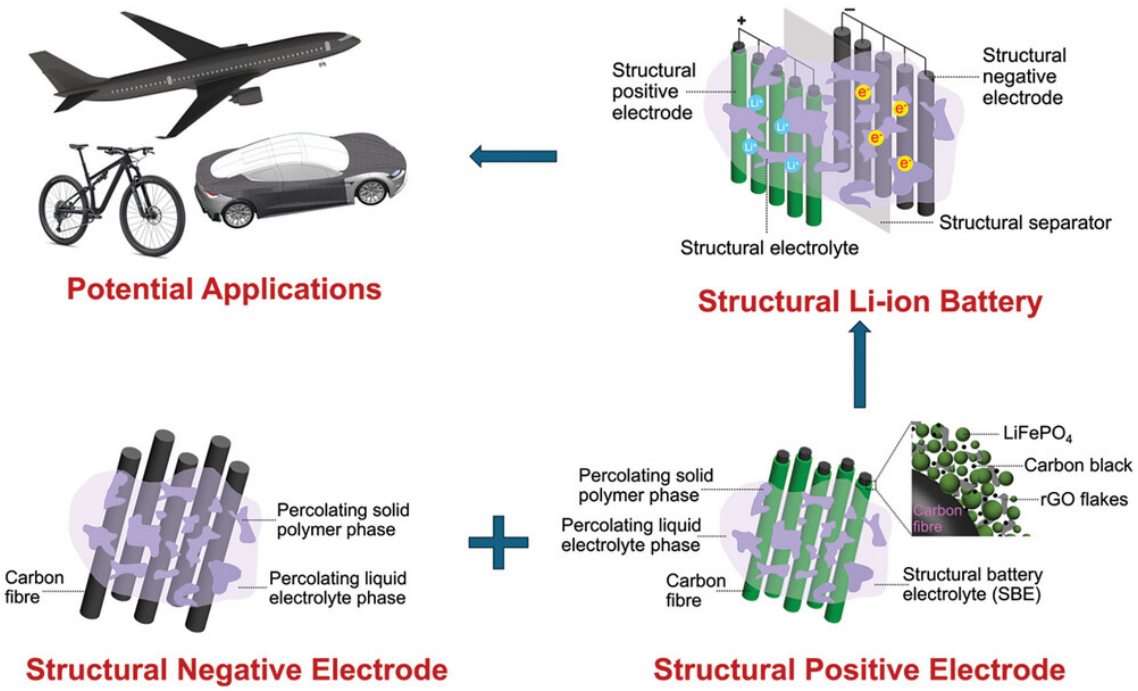

Figure 3.1: A detailed roadmap for the development and implementation of All-Fiber Structural Batteries. Reproduced from Chaudhary et al. [5].

The concept of multifunctionality is central to structural batteries. Multifunctionality means that a single material or component performs multiple engineering functions simultaneously rather than requiring separate components for each function. In the case of structural batteries, the multifunctionality combines two primary functions: electrochemical energy storage (like a conventional battery) and mechan-

ical load-bearing capability (like structural materials such as aluminum or steel). This dual functionality eliminates the need for separate battery housing and structural framework, potentially reducing overall system weight and volume. The key advantage lies in replacing "dead weight" components that only provide structure with "active" components that provide both structure and energy storage, leading to more efficient use of materials and space in weight-critical applications such as vehicles, aircraft, or portable electronics.

3.2 Electrochemistry of Batteries

Battery operation fundamentally relies on electrochemical processes that convert chemical energy into electrical energy through controlled redox reactions. A battery consists of four essential components: the anode (negative electrode), cathode (positive electrode), electrolyte, and separator (Figure 3.2). During discharge, oxidation occurs at the anode where electrons are released, while reduction takes place at the cathode where electrons are consumed. The electrolyte facilitates ionic transport between electrodes while remaining electronically insulating, forcing electrons to travel through an external circuit to complete the electrochemical reaction and generate useful electrical current. The separator prevents direct contact between electrodes while allowing ion passage, maintaining charge balance and preventing short circuits.

Key performance parameters define battery effectiveness and include voltage, capacity, efficiency, and cycling stability. The cell voltage results from the potential difference between anode and cathode, determined by their respective electrochemical potentials and the thermodynamics of the redox reactions. Capacity represents the total charge storage capability, typically expressed in ampere-hours (Ah) or milliampere-hours per gram (mAh/g) for specific capacity. Coulombic efficiency measures the ratio of discharge to charge capacity, indicating the reversibility of electrochemical processes, while cycling stability quantifies capacity retention over repeated charge-discharge cycles, reflecting the long-term viability of the battery system.

The conversion of chemical energy to electrical energy in batteries is governed by fundamental thermodynamic principles that determine both theoretical limits and practical performance [11]. The maximum voltage achievable by a battery is dictated by the Gibbs free energy change (ΔG) of the overall redox reaction, related to cell potential through the equation $\Delta G = -nFE$, where n is the number of electrons transferred, F is Faraday's constant (96,485 C mol^{-1}), and E is the cell potential [17]. However, actual energy output is influenced by kinetic factors such as activation overpotentials, concentration gradients, and ohmic losses within the cell [15]. Temperature plays a critical role in battery performance, as lower temperatures reduce both cell voltage and internal diffusion rates of ions, while elevated temperatures can accelerate unwanted side reactions and electrolyte degradation [16]. The rate at which current can be drawn from a battery is ultimately limited by the diffusion rates of ionic species through the electrolyte, establishing fundamental

constraints on power delivery capabilities.

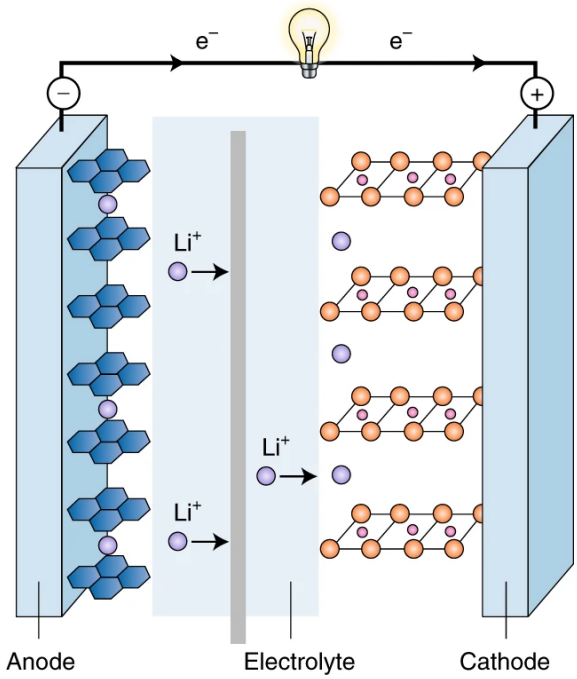

Figure 3.2: Components of a rechargeable Li-ion battery showing the main structural elements and their functions. Reproduced from Goodenough [21].

3.3 PTMA

Poly(2,2,6,6-tetramethylpiperidinyloxy-4-yl methacrylate) (PTMA) represents a pioneering achievement in organic radical battery technology, first demonstrated as a viable rechargeable battery cathode material by Nakahara et al. in 2002 [20]. This groundbreaking work at NEC Corporation revealed that nitroxide radical polymers could achieve reversible electrochemical cycling with remarkable stability. PTMA features a methacrylate polymer backbone with pendant 2,2,6,6-tetramethyl piperidinyloxy (TEMPO) groups that serve as electroactive centers (Figure 3.3). The TEMPO moiety contains a stable nitroxide radical (N-O$^{\bullet}$) that undergoes reversible one-electron oxidation to an oxoammonium cation (N-O^{+}) according to the reaction:

$$\text{TEMPO} + \text{A}^- \rightleftharpoons \text{TEMPO}^+ + \text{A}^- + \text{e}^- \tag{3.1}$$

where A^- represents the electrolyte anion. This mechanism involves anion insertion/extraction rather than cation intercalation, distinguishing PTMA from conventional inorganic cathodes and enabling exceptionally fast kinetics due to the surface-localized nature of the redox reaction.

PTMA synthesis typically employs free radical polymerization of the 4-methacryloyl oxy-TEMPO monomer using conventional initiators such as AIBN. Copolymerization with comonomers such as glycidyl methacrylate (GMA) introduces crosslinking

capabilities through epoxide groups, enhancing mechanical properties while maintaining electrochemical activity [9]. PTMA offers several compelling advantages as a cathode material: environmental sustainability through earth-abundant elements (C, H, N, O) with no conflict minerals, high power capability enabling stable cycling at rates up to 25C, processing flexibility due to good solubility in organic solvents, and excellent thermal stability. The theoretical specific capacity of 111 mAh g^{-1} based on one-electron transfer per TEMPO unit, combined with operating potentials of 3.6–3.8 V versus Li/Li^+, makes PTMA particularly attractive for structural battery applications where simultaneous energy storage and load-bearing capabilities are required.

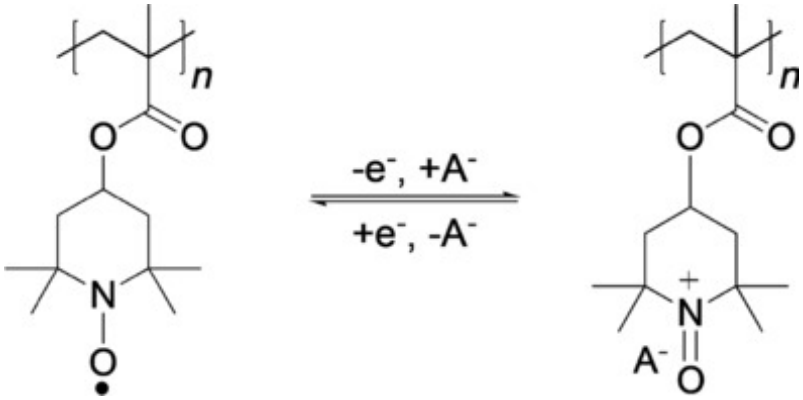

Figure 3.3: Reversible redox mechanism of PTMA showing the one-electron transfer between neutral nitroxide radical (N-O$^\bullet$) and oxoammonium cation (N-O$^+$) states, with anion insertion/extraction (A^-) for charge balance during battery operation. Reproduced from Wang et al. [9].

3.4 Electrochemical Characterization Techniques

3.4.1 Cyclic Voltammetry

Cyclic voltammetry (CV) is a very useful technique that provides deep insight about the thermodynamic and kinetic properties of redox-active materials. The technique involves applying a voltage waveform to the electrode while recording the resulting current response.

3.4.1.1 Fundamental Principes

In cyclic voltammetry, the potential is swept linearly from an initial value to an already set limit, then reversed and swept back to the initial potential. This creates a special current-voltage profile that reveals the electrochemical behavior of the active material. The resulting voltammogram exhibits distinct anodic and cathodic peaks corresponding to oxidation and reduction processes, respectively [12].
For a simple one-electron transfer reaction:

$$O + e^- \rightleftharpoons R \tag{3.2}$$

Where, O is the oxidised species, which on gaining one electron becomes the reduced species and it is reversible.

The Nernst equation describes the thermodynamic relationship between electrode potential and the concentrations of redox species in solution. For a general redox reaction of the form $\mathrm{Ox} + ne^- \rightleftharpoons \mathrm{Red}$, the electrode potential E is given by:

$$E = E^0 + \frac{RT}{nF} \ln \left(\frac{[\mathrm{Ox}]}{[\mathrm{Red}]} \right) \tag{3.3}$$

where E^0 is the standard electrode potential, R is the gas constant (8.314 J mol^{-1} K^{-1}), T is the absolute temperature, n is the number of electrons transferred, F is Faraday's constant (96,485 C mol^{-1}), and [Ox] and [Red] are the concentrations of the oxidized and reduced species, respectively. At 25°C, the equation simplifies to $E = E^0 + \frac{0.0592}{n} \log \left(\frac{[\mathrm{Ox}]}{[\mathrm{Red}]} \right)$ when using base-10 logarithms. This fundamental relationship is essential in electrochemistry as it allows prediction of electrode potentials under non-standard conditions. The equation also governs the peak potentials observed and explains how experimental conditions such as concentration and pH can change the potential of active material.

The peak current for a reversible system is described by the Randles-Sevcik equation:

$$i_p = 2.69 \times 10^5 n^{3/2} A D^{1/2} C v^{1/2} \tag{3.4}$$

where i_p is the peak current (A), n is the number of electrons transferred, A is the electrode area (cm^2), D is the diffusion coefficient (cm^2/s), C is the bulk concentration (mol/cm^3), and v is the scan rate (V/s) [13].

3.4.1.2 Reversibility Determination

The degree of how much the electrochemistry is reversible is a critical parameter that highlights the electron transfer abilities and the presence of associated reactions. The assessment is primarily based on the peak-to-peak separation (ΔE_p) and the peak current ratio [14].

3.4.1.3 Reversible Systems

For an electrochemically reversible system at 25°C, the theoretical criteria are:

- Peak separation: $\Delta E_p = \frac{59 \text{ mV}}{n}$ (not depends on scan rate)
- Peak current ratio: $\left| \frac{i_{pa}}{i_{pc}} \right| = 1$
- Peak current proportional to $v^{1/2}$
- Formal potential: $E^{0\prime} = \frac{E_{pa} + E_{pc}}{2}$

3.4.1.4 Classification Criteria

The electrochemical reversibility is classified based on the peak separation [15]:

- **Reversible**: $\Delta E_p \leq 59$ mV for single-electron transfer
- **Quasi-reversible**: $59 < \Delta E_p \leq 100$ mV
- **Irreversible**: $\Delta E_p > 100$ mV

3.4.1.5 Significance

Reversible systems indicate fast electron transfer activity. These systems exhibit Nernstian behavior and are ideal for applications requiring efficient charge transfer, such as in energy storage devices [16].

Quasi-reversible systems demonstrate moderate electron transfer rates. The peak separation increases with scan rate, reflecting finite electron transfer rate constants.

Irreversible systems are characterized by slow electron transfer kinetics, often accompanied by coupled chemical reactions or significant activation barriers. These systems show scan rate-dependent peak potentials and may exhibit only one observable peak at moderate scan rates [17].

3.4.1.6 Quantitative Analysis

The formal potential ($E^{0'}$) represents the thermodynamic driving force for the redox system and is calculated as:

$$E^{0'} = \frac{E_{pa} + E_{pc}}{2} \tag{3.5}$$

For reversible systems, this value is independent of scan rate and provides insight into the relative stability of the oxidized and reduced forms [18].
The peak current ratio provides information about the chemical stability of the electrogenerated species and the presence of follow-up chemical reactions:

$$\frac{|i_{pa}|}{|i_{pc}|} = 1 \text{ (reversible, no side reactions)} \tag{3.6}$$

Deviations from unity indicate either irreversible electron transfer or coupled chemical processes such as dimerization, protonation, or decomposition reactions [19].

3.4.2 Galvanostatic Charge Discharge

Galvanostatic Charge Discharge is a widely used technique for battery characterization that combines constant current with voltage limitations to ensure safe and controlled testing setups. In GCD, the battery is cycled between fixed voltage limits ($V_{\max}$ and $V_{\min}$) under constant current, thereby allowing for a decent evaluation of electrochemical performance, capacity, and cycleability. The technique works by applying a constant current I during charging and discharging phases, with the relationship between current, capacity, and time given by:

$$Q = \int_0^t I \, dt = I \cdot t \quad \text{(for constant current)} \tag{3.7}$$

where Q is the accumulated charge capacity, I is the applied current, and t is the time duration. The specific capacity is calculated as $Q_{\text{sp}} = Q/m$, where m is the active material mass.

3.4.2.1 C-Rate and its Effects on Battery Performance

The C-rate is a fundamental parameter in battery testing that defines the charge or discharge current relative to the battery's theoretical capacity, expressed as:

$$\text{C-rate} = \frac{I}{Q_{\text{nominal}}} \tag{3.8}$$

where I is the applied current and Q_{nominal} is the nominal capacity of the battery. A 1C rate corresponds to a current that would theoretically charge or discharge the battery in one hour, while 0.1C and 10C rates correspond to 10-hour and 6-minute durations, respectively. The C-rate significantly affects battery performance through several mechanisms: at higher C-rates, increased polarisation losses lead to reduced available capacity due to kinetic limitations and resistance.

3.4.2.2 Specific Capacity

Specific capacity represents the amount of electrical charge that can be stored per unit mass of active material, serving as a fundamental metric for evaluating electrode performance. For battery applications, specific capacity is typically expressed in milliampere-hours per gram (mAh g^{-1}) and is calculated using:

$$Q_{\text{sp}} = \frac{Q}{m_{\text{active}}} = \frac{\int_{t_1}^{t_2} I\, dt}{m_{\text{active}}} \tag{3.9}$$

where Q_{sp} is the specific capacity (mAh g^{-1}), Q is the total charge passed (mAh), I is the current (mA), and m_{active} is the mass of active material (g). For PTMA-based electrodes, the theoretical specific capacity is 111 mAh g^{-1}, calculated from the molecular weight and one-electron transfer per TEMPO unit according to:

$$Q_{\text{theoretical}} = \frac{n \times F}{M_w \times 3.6} \tag{3.10}$$

where n is the number of electrons transferred per molecule (1 for PTMA), F is Faraday's constant (96,485 C mol^{-1}), M_w is the molecular weight of the repeating unit (241.3 g mol^{-1} for PTMA), and 3.6 is the conversion factor from C g^{-1} to mAh g^{-1}.

3.4.2.3 Capacity Retention

Capacity retention quantifies the cycling stability of an electrode material by measuring the percentage of initial capacity maintained after repeated charge-discharge cycles. This parameter is crucial for assessing the long-term viability of battery systems and is calculated as:

$$\text{Capacity Retention (\%)} = \frac{Q_{\text{cycle,n}}}{Q_{\text{cycle,initial}}} \times 100 \tag{3.11}$$

where $Q_{\text{cycle,n}}$ is the discharge capacity at cycle n and $Q_{\text{cycle,initial}}$ is the discharge capacity of the first cycle (or a reference cycle after formation). High capacity retention (>80% after hundreds of cycles) indicates stable electrochemical processes

with minimal degradation mechanisms such as active material dissolution, structural changes, or side reactions.

3.4.2.4 Coulombic Efficiency

Coulombic efficiency (CE) measures the reversibility of charge storage and is defined as the ratio of discharge capacity to charge capacity for each cycle. This parameter indicates the presence of irreversible side reactions and is fundamental for evaluating battery performance:

$$\eta_{\mathrm{CE}} = \frac{Q_{\mathrm{discharge}}}{Q_{\mathrm{charge}}} \times 100\% \tag{3.12}$$

where η_{CE} is the coulombic efficiency (%), $Q_{\mathrm{discharge}}$ is the capacity delivered during discharge (mAh), and Q_{charge} is the capacity consumed during charge (mAh). Ideal systems exhibit coulombic efficiencies approaching 100%, indicating complete charge recovery with minimal parasitic reactions. For PTMA-based systems, high coulombic efficiency (>95%) demonstrates the reversible nature of the nitroxide radical redox reaction and minimal electrolyte decomposition or active material dissolution.
The cumulative coulombic efficiency over multiple cycles can be calculated as:

$$\eta_{\mathrm{cumulative}} = \prod_{i=1}^{n} \frac{Q_{\mathrm{discharge,i}}}{Q_{\mathrm{charge,i}}} \tag{3.13}$$

This metric provides insight into long-term charge retention and helps identify gradual capacity fade mechanisms that may not be apparent from single-cycle measurements.

4
Methodology

This chapter delves into the precise methodology adopted for synthesis, characterization, analysis and mechanical testing of the PTMA-coated carbon fibers.

4.1 Synthesis

The synthesis of electroactive PTMA-co-GMA followed a two-step free radical polymerization methodology, as illustrated in Figure 4.1. This approach was selected after unsuccessful attempts with anionic polymerization methods, which failed due to the harsh reaction conditions required and the hygroscopic nature of the TEMPO-containing monomers that compromised the stringent moisture-free environment necessary for living anionic polymerization.

4.1.1 Step 1: Free Radical Copolymerization

PTMPM-co-GMA copolymer was synthesized via free radical polymerization using 4-methacryloyloxy-2,2,6,6-tetramethylpiperidine (TMPM, TCI Chemicals, Tokyo) and glycidyl methacrylate (GMA, ≥97.0% GC, Sigma-Aldrich) as co-monomers. The reaction mixture contained TMPM (22 mmol, 5.0 g), varying amounts of GMA (1–5 mol%), and azobisisobutyronitrile (AIBN, 0.67 mmol, 0.109 g) as the radical initiator in anhydrous toluene (10 mL) solvent.

The polymerization was conducted at 60°C for 48 hours under nitrogen atmosphere to prevent oxygen inhibition of the radical process (Figure 4.2a). AIBN was selected as the initiator due to its clean decomposition mechanism, which generates two 2-cyanoprop-2-yl radicals and nitrogen gas at temperatures above 40°C, avoiding oxygenated byproducts that could interfere with the electrochemical properties. The reaction yielded approximately 85% of a clear, viscous copolymer that remained soluble in common organic solvents including chloroform and toluene (Figure 4.2b).

4.1.2 Step 2: Oxidation to Nitroxide Radicals

The electrochemically inactive PTMPM-co-GMA was converted to electroactive PTMA-co-GMA through oxidation using meta-chloroperoxybenzoic acid (mCPBA, ≤77%, Sigma-Aldrich) as the oxidizing agent (Figure 4.2c-d). The copolymer was treated with 2 equivalents of mCPBA for 3 hours at room temperature, converting the TEMPO NH groups to active nitroxide radicals (N-O$^{\bullet}$). This oxidation step typically achieved 65–81% radical conversion. The oxidation yield was approximately

50%, consistent with literature reports for mCPBA oxidation of TEMPO-containing polymers (Figure 4.2e-f).

4.1.3 Material Sourcing and Quality Control

All chemicals were used as received without further purification. TMPM was sourced from Tokyo Chemical Industry (TCI) due to their high-purity specialty chemical portfolio. GMA (≥97.0% GC purity) and mCPBA (≤77% active oxygen content) were obtained from Sigma-Aldrich. AIBN was available from the composite laboratory stock. The choice of high-purity starting materials was critical for achieving reproducible electrochemical performance and minimizing side reactions during both polymerization and oxidation steps.

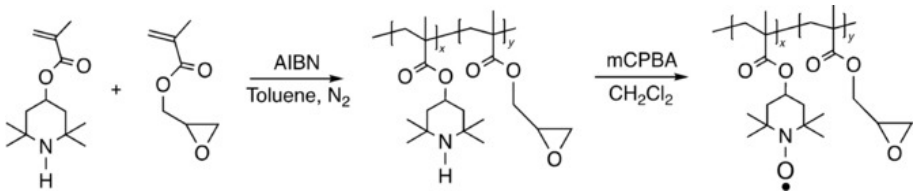

Figure 4.1: Synthesis scheme for PTMA-co-GMA copolymer showing (a) free radical polymerization of TMPM and GMA monomers and (b) oxidation of PTMPM-co-GMA to electroactive PTMA-co-GMA using mCPBA. Adapted from Wang et al. [9].

4.1.4 Failed Synthesis Approaches

Initial attempts using anionic polymerization techniques, following protocols similar to those reported by Vetter et al. [10], were unsuccessful. The failure was attributed to two primary factors, one being the harsh reaction conditions required for anionic polymerization (such as high vacuum and extremely dry conditions) were incompatible with the TEMPO-containing monomers, and secondly, the hygroscopic nature of PTMA Free radical compromised the moisture-free environment essential for controlled anionic polymerization. These challenges led to the adoption of the more robust free radical polymerization approach that demonstrated excellent tolerance to trace moisture and ambient conditions.

4.2 Electrode Fabrication

4.2.1 Carbon Fiber Substrate Preparation

T800-50SC-12K carbon fibers from Toray, which had been spread to a 15 mm width by Oxeon AB, were cut to 60 mm lengths to match the dimensions of microscopy glass slides, providing a standardized substrate for electrode fabrication. To ensure optimal polymer adhesion and remove commercial sizing agents, the carbon fiber substrates underwent desizing treatment using Soxhlet extraction with acetone for 18 hours. This process eliminated surface contaminants and activated the fiber surface for improved polymer-substrate interaction.

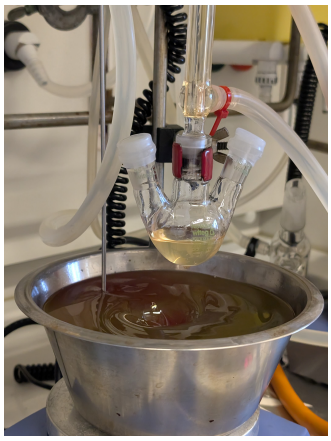

(a) Initial reaction setup

(b) Polymerization product

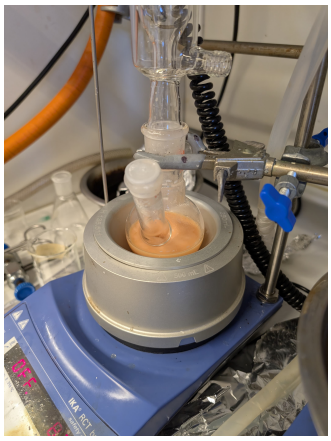

(c) mCPBA oxidation

(d) Intermediate product

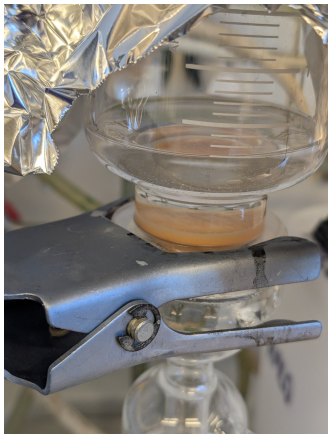

(e) Final PTMA-co-GMA

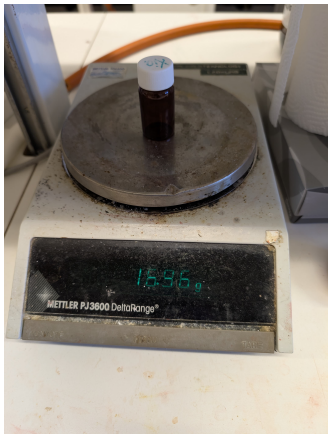

(f) Ready for characterization

Figure 4.2: Experimental photographs showing key stages of PTMA-co-GMA synthesis: (a) reaction setup with nitrogen atmosphere, (b) clear viscous copolymer after polymerization, (c) mCPBA oxidation process, (d) intermediate product, (e) final electroactive PTMA-co-GMA, and (f) product ready for characterization.

4.2.2 Slurry Formulation and Preparation

The electrode slurry was formulated using a four-component system designed to optimize both electrochemical performance and processability. PTMA-co-GMA served as the active material, providing the primary electrochemical energy storage capability through its rapid redox-active nitroxide groups. PVDF was incorporated as a polymeric binder to ensure mechanical integrity and adhesion between the active material and the carbon fiber substrate. The conductive additive system comprised both reduced graphene oxide (rGO) and carbon black, which collectively enhanced electronic conductivity throughout the electrode. In addition to its conductivity benefits, rGO contributed significantly to the electrode's surface area, providing additional pathways for ion transport and improving the electrochemical accessibility of the active material[6].

The slurry preparation followed a carefully controlled mixing protocol to ensure uniform dispersion and prevent agglomeration. Initially, PVDF, rGO, and carbon black were dispersed in N-methyl-2-pyrrolidone (NMP) and subjected to sonication to achieve optimal dispersion of the conductive network. Subsequently, crystalline PTMA-co-GMA was dissolved separately in NMP to form a homogeneous solution before being combined with the pre-dispersed mixture. The final blending was achieved through planetary mixing, ensuring thorough integration of all components while maintaining the integrity of the conductive pathways.

4.2.3 Design of Experiments

A systematic design of experiments was implemented with five distinct formulations, with each slurry preparation totaling 300 mg.

Formulation ID	**PTMA-co-GMA (wt%)**	**Carbon Black (wt%)**	**PVDF (wt%)**	**rGO (wt%)**
F1	30	40	20	10
F2	45	30	15	10
F3	60	25	10	5
F4	60	20	20	–
F5	60	–	20	20

Table 4.1: Electrode formulation matrix. F4 excludes rGO, F5 excludes carbon black.

Each formulation was prepared in quadruplicate, resulting in 20 samples designated SS01–SS20:

- F1: SS01–SS04
- F2: SS05–SS08
- F3: SS09–SS12
- F4: SS13–SS16 (without rGO)
- F5: SS17–SS20 (without carbon black)

4.2.4 Coating and Thermal Processing

The prepared slurries were applied to desized carbon fiber substrates using hand doctor blading. Following coating application, the electrodes underwent thermal processing in a Büchi oven at 175°C for 3 hours to achieve dual objectives. This thermal treatment first ensured complete removal of the N-methyl-2-pyrrolidinone (NMP) solvent, preventing any residual solvent interference with electrochemical performance. Simultaneously, the elevated temperature initiated GMA epoxide crosslinking reactions, forming a three-dimensional polymer network that prevents dissolution of the active material during electrochemical cycling. This thermal crosslinking approach has been demonstrated to retain over 70% of the original nitroxide radical content while providing mechanical stability and solvent resistance to the electrode [9] coating.

4.2.5 Mass Loading Results

Post-thermal treatment mass loadings were determined gravimetrically for all samples and normalized by electrode area (9 cm^2).

F1		**F2**		**F3**		**F4**		**F5**	
ID	**mg/cm²**	**ID**	**mg/cm²**	**ID**	**mg/cm²**	**ID**	**mg/cm²**	**ID**	**mg/cm²**
SS01	1.711	SS05	0.689	SS09	1.550	SS13	1.250	SS17	1.254
SS02	1.322	SS06	0.933	SS10	2.162	SS14	1.370	SS18	0.928
SS03	0.600	SS07	1.129	SS11	1.203	SS15	2.024	SS19	0.997
SS04	0.571	SS08	1.036	SS12	1.491	SS16	1.173	SS20	1.580
Avg	**1.051**	**Avg**	**0.947**	**Avg**	**1.602**	**Avg**	**1.454**	**Avg**	**1.190**

Table 4.2: Mass loadings per unit area (mg/cm^2) after thermal crosslinking at 175°C for 3 hours. Electrode dimensions: 15 mm × 60 mm (9 cm^2).

4.3 Half Cell Assembly

Half cell assembly was conducted in the composite laboratory using flexible pouch cell packaging composed of a laminated film consisting of polyethylene terephthalate (PET), aluminum (Al), and polyethylene (PE) layers with thicknesses of 12 μm, 9 μm, and 75 μm respectively. The pouch cells, when folded, measured 8.5 cm by 8.5 cm, providing sufficient space for electrode and electrolyte containment while maintaining compact dimensions suitable for electrochemical testing.

The current collector configuration employed a dual-metal approach, with aluminum strips serving as the positive current collectors due to their excellent electrical conductivity and chemical stability, and nickel strips used as negative current collectors optimized for compatibility with lithium metal electrodes.

Prior to cell assembly, the thermally crosslinked PTMA-co-GMA electrodes were integrated with the current collectors. Aluminum strips were positioned between the carbon fiber substrate and the glass slide, and Pelco conductive carbon adhesive was

applied to ensure optimal electrical contact between the aluminum current collector and the carbon fiber electrode. This assembly was then cured at 150°C for 2 hours to complete adhesive polymerization and establish reliable electrical pathways.

The half cell assembly procedure involved carefully excising the carbon fiber electrode from the glass substrate and positioning it within the pouch cell cavity. A Whatman microfiber separator was placed over the electrode to prevent direct contact between the positive and negative electrodes. Nickel strips were positioned to facilitate connection with lithium metal counter electrodes during subsequent glovebox operations. The pouch was temporarily heat-sealed at the top and sides, leaving the bottom opening accessible for glovebox manipulation. To prevent short circuits and ensure safe handling during assembly, white tape and Kapton tape were applied as insulation measures.

To remove residual solvents and moisture that could interfere with electrochemical performance, the partially assembled cells were placed in a vacuum oven overnight, ensuring optimal electrolyte uptake and preventing unwanted side reactions.

Final assembly was completed in an inert atmosphere glovebox, where 1M lithium bis(trifluoromethanesulfonyl)imide (LiTFSI) in ethylene carbonate:propylene carbonate (EC:PC) at a 1:1 weight ratio was dispensed onto the separator. Two to three lithium metal coin electrodes were positioned as the negative electrode, and the pouch cell was vacuum-sealed to create an airtight environment suitable for electrochemical testing.

This half cell design enables systematic evaluation of PTMA-co-GMA electrode performance while providing a controlled environment for electrochemical characterization.

4.4 Electrochemical Testing

4.4.1 Cyclic Voltammetry

Cyclic voltammetry measurements were performed using a Biologic BCS805 potentiostat/galvanostat system, which provided precise control over the applied potential and accurate current measurements throughout the voltage scanning process. The cyclic voltammetry experiments were conducted with carefully optimized parameters to ensure accurate characterization of the PTMA-based electrodes. A scan rate of 0.1 mV/s was selected to maintain quasi-equilibrium conditions and achieve clear resolution of redox peaks. The initial potential was set at 2.6 V versus Li/Li^+, with the voltage window spanning from 2.6 V to 4.2 V versus Li/Li^+ to encompass the expected redox activity of PTMA. The vertex potentials were established with an upper limit of 4.2 V and a lower limit of 2.6 V versus Li/Li^+. Five complete oxidation-reduction cycles were performed to assess the reversibility and stability of the electrochemical response.

Current sampling employed a specialized protocol where current values were recorded and averaged over the last 50% of each potential step duration to minimize transient effects and ensure steady-state measurements. Data acquisition settings involved

averaging current measurements over 20 voltage steps using a fast bandwidth configuration to enhance the signal-to-noise ratio. The final scan was terminated at 2.6 V versus Li/Li^+ to complete the electrochemical characterization cycle.

The resulting cyclic voltammograms were systematically analyzed to extract key electrochemical parameters that provide insight into the electrode performance. Analysis focused on determining the oxidation and reduction peak potentials (E_{pa} and E_{pc}), peak current densities (i_{pa} and i_{pc}), and peak separation ($\Delta E_p = E_{pa} - E_{pc}$) as an indicator of electrochemical reversibility. The current ratio (i_{pa}/i_{pc}) was calculated to assess redox symmetry, while cycling stability was evaluated through comparison of successive cycles to identify any degradation or capacity fade.

All electrochemical measurements were conducted at room temperature (approximately 25°C) under controlled environmental conditions to ensure reproducible results. All potentials reported in this study are referenced to the Li/Li^+ electrode to maintain consistency with standard electrochemical practices for lithium battery research.

Cycle Selection Methodology

The selection of the most representative cycle from the five recorded cycles was critical for accurate performance comparison across samples. A composite scoring algorithm was developed based on three electrochemical criteria:

$$\text{Cycle Score} = 0.5 \times S_{\text{rev}} + 0.3 \times S_{\text{bal}} + 0.2 \times S_{\text{mag}} \tag{4.1}$$

where:

$$S_{\text{rev}} = \frac{1}{\Delta E_p + 0.001} \quad \text{(Reversibility score)} \tag{4.2}$$

$$S_{\text{bal}} = \frac{1}{|I_{pa}/I_{pc} - 1| + 0.001} \quad \text{(Charge balance score)} \tag{4.3}$$

$$S_{\text{mag}} = \frac{I_{\text{peak}}}{I_{\text{max,all}}} \quad \text{(Current magnitude score)} \tag{4.4}$$

The weighting factors prioritize electrochemical reversibility (50%), followed by charge balance (30%), and current magnitude (20%). This approach ensures selection of cycles exhibiting optimal kinetics while avoiding degraded or anomalous behavior. Systematic application across all samples consistently identified cycles 2–3 as optimal, avoiding initial activation effects observed in the first cycle and later degradation phenomena that became apparent in cycles 4–5.

Data analysis revealed that this methodology was particularly crucial for samples showing significant performance drift over cycling, such as SS09 and SS10, where individual cycles varied dramatically in their electrochemical characteristics.

4.4.2 Galvanostatic Charge-Discharge Testing

Galvanostatic charge-discharge measurements were performed using a Bio-Logic BCS805 potentiostat/galvanostat system to evaluate the electrochemical perfor-

mance and rate capability of PTMA-co-GMA composite electrodes. The half-cell configuration employed lithium metal as both counter and reference electrodes.

The experimental protocol was designed to systematically assess rate capability through sequential testing at multiple C-rates, specifically 0.1C, 0.2C, 0.5C, 1C, and 2C, with each rate maintained for five complete charge-discharge cycles. This progression from quasi-equilibrium conditions at 0.1C to high-rate cycling at 2C enabled comprehensive evaluation of both capacity retention and kinetic limitations. The theoretical capacity of PTMA (111 mAh g^{-1}) and gravimetrically determined active material mass loading were used to calculate appropriate current densities for each C-rate.

A voltage window of 3.4 V to 3.8 V versus Li/Li^+ was selected based on preliminary cyclic voltammetry results that identified the primary TEMPO redox activity within this range. This narrow potential window ensured complete utilization of the PTMA electrochemical activity while preventing electrolyte degradation at high potentials and avoiding lithium plating at low potentials, thereby optimizing cycling stability for long-term performance evaluation.

Each testing sequence began with three formation cycles to stabilize the electrode-electrolyte interface and establish reproducible electrochemical behavior. Data acquisition was managed through EC-Lab software interfaced with the Bio-Logic system, recording current and voltage measurements. The comprehensive dataset enabled calculation of specific capacity as the ratio of accumulated charge to PTMA mass loading, coulombic efficiency as the percentage ratio of discharge to charge capacity. All experimental data collected through EC-Lab were subsequently processed and visualized using MATLAB software to generate publication-quality plots and perform statistical analysis of cycling performance metrics.

5

Results

This chapter systematically presents the experimental findings that characterize the synthesized PTMPM-*co*-GMA copolymer and its electroactive oxidized PTMA-*co*-GMA derivative. The investigation employed complementary analytical techniques to thoroughly examine the structural, morphological, and electrochemical properties of these materials.

The research methodology encompassed three primary analytical approaches. Spectroscopic analysis utilized FTIR, $^{1}H/^{13}C$ NMR, and GPC techniques to confirm the chemical structure and verify successful oxidation of the polymer. Morphological analysis employed SEM to assess coating integrity and evaluate the effects of crosslinking on the material's physical structure. Electrochemical analysis incorporated CV, and GCD methods to evaluate redox activity, characterize charge transfer kinetics, and assess overall battery performance characteristics.

Through the integration of these diverse analytical methods, the study provides a comprehensive understanding of the material's fundamental properties and establishes its suitability for structural battery applications. This multi-faceted approach ensures that both the chemical composition and functional performance of the copolymer system are thoroughly characterized and validated.

5.1 Spectroscopic Analysis- HNMR and CNMR

Nuclear magnetic resonance spectroscopy was performed by the Chemistry Department at Chalmers University of Technology to characterize the PTMPM-co-GMA copolymer before and after oxidation to the electroactive PTMA-co-GMA form.

5.1.1 PTMPM-co-GMA (NH Form):

The ^{1}H NMR spectrum (Figure 5.1a) confirmed successful copolymer synthesis with the TEMPO ester-bearing proton at δ = 5.07–5.08 ppm (LW = 1.02 Hz), backbone CH_2 at δ = 1.88 ppm, TEMPO ring CH_2 at δ = 2.05 ppm, and overlapping methyl signals at δ = 1.0–1.3 ppm. These assignments are consistent with the ^{1}H NMR data reported in the supporting information of Wang et al., confirming the structural similarity of the PTMPM-co-GMA precursor material [9]. The ^{13}C NMR spectrum (Figure 5.1b) showed ester carbonyls at δ = 177.41 and 176.13 ppm, TEMPO carbons at δ = 69.79 (ester-bearing), 34.92 (quaternary), and 29.05 ppm (methyls), GMA epoxide carbons at δ = 45.41 and 54.24 ppm, and backbone carbons

at $\delta = 51.47$ and 43.48 ppm.

5.1.2 PTMA-co-GMA (N-O$^\bullet$ Form):

After mCPBA oxidation, the ^{1}H NMR spectrum (Figure 5.1c) exhibited characteristic paramagnetic effects with TEMPO methyls shifting to δ 0.24 and 1.43 ppm, and a broad envelope at δ 2.0–2.5 ppm representing severely broadened polymer protons. Additionally, new signals appeared in the δ 3.0–4.5 ppm region, indicating epoxide ring opening during the oxidation process. These peaks correspond to CH-OH (δ 3.6–4.2 ppm) and CH_2-OH (δ 3.4–3.8 ppm) protons from ring-opened GMA units, confirming that mCPBA not only oxidizes TEMPO groups but also attacks the epoxide functionality. The TEMPO ester proton disappeared due to paramagnetic broadening. Aromatic signals at δ 7.6–8.2 ppm confirmed *m*-chlorobenzoic acid byproduct formation.

5.1.3 Oxidation Confirmation:

The dramatic spectral changes including paramagnetic line broadening, chemical shift alterations, and signal intensity reductions provide definitive evidence of successful NH $\rightarrow$ N-O$^\bullet$ oxidation, converting the inactive PTMPM-co-GMA to electroactive PTMA-co-GMA while preserving structural integrity for structural battery applications.

5.2 Spectroscopic Analysis- FTIR

FTIR spectroscopy was employed to confirm the successful synthesis of PTMA-co-GMA copolymer and verify the preservation of critical functional groups following thermal crosslinking at 175°C for 3 hours. Figure 5.2 presents the complete FTIR spectrum with key peak assignments, while Figure 5.3 provides detailed molecular structure correlations.

5.2.1 Critical Peak Identification

The FTIR spectrum exhibits several characteristic absorption bands that confirm the successful incorporation of both PTMA and GMA components, as illustrated in Figures 5.2 and 5.3:

Ester Carbonyl Region (1740 cm^{-1}): A strong, sharp absorption peak at 1740 cm^{-1} corresponds to the C=O stretching vibration of ester groups present in both PTMA and GMA monomeric units. The intensity and sharpness of this peak indicate excellent structural integrity of the polymer backbone following thermal treatment.

TEMPO Radical Region (1375 cm^{-1}): The distinct absorption at 1375 cm^{-1} is attributed to the N-O stretching vibration of TEMPO radicals. The presence and intensity of this peak is critical as it confirms the preservation of electroactive sites essential for battery functionality. This peak demonstrates that the thermal

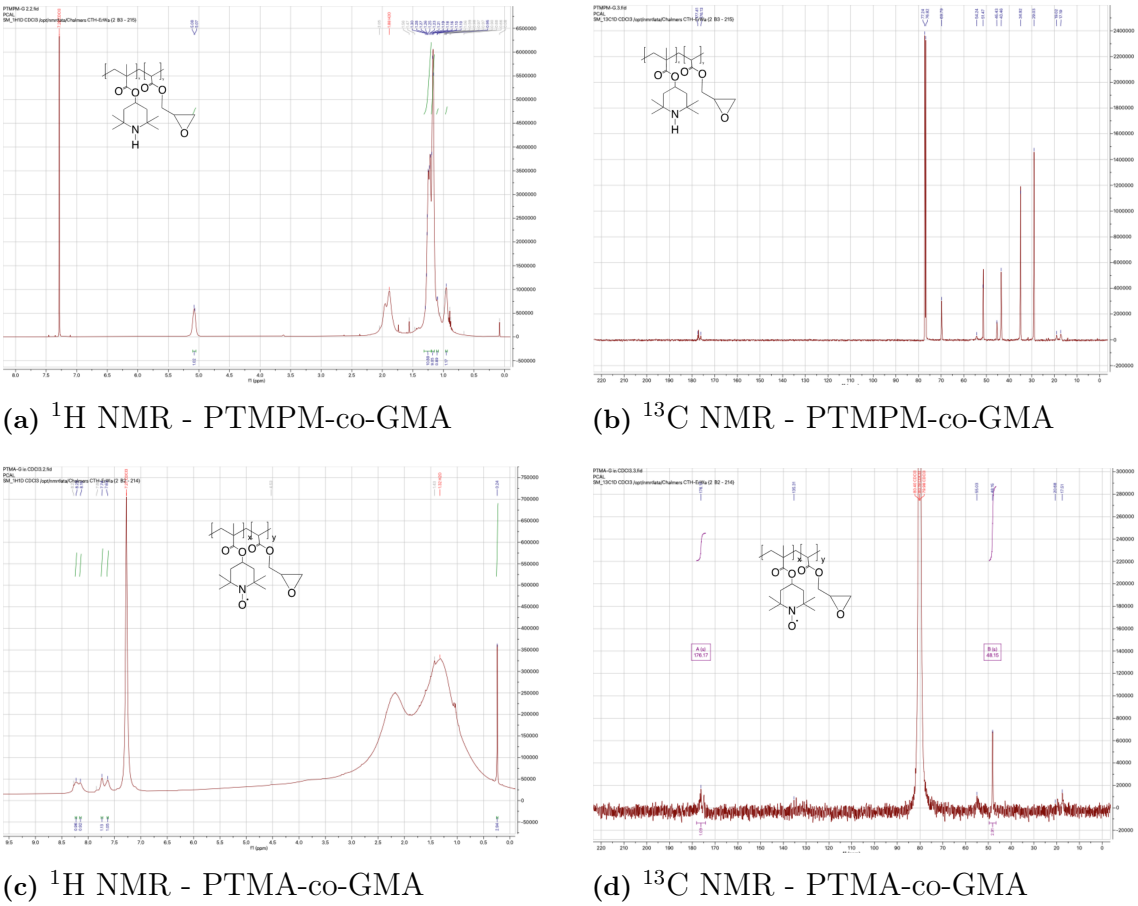

(a) ^{1}H NMR - PTMPM-co-GMA

(b) ^{13}C NMR - PTMPM-co-GMA

(c) ^{1}H NMR - PTMA-co-GMA

(d) ^{13}C NMR - PTMA-co-GMA

Figure 5.1: NMR spectroscopic characterization of PTMPM-co-GMA before (a,b) and after (c,d) mCPBA oxidation to PTMA-co-GMA.

crosslinking conditions (175°C, 3h) successfully maintained the radical character necessary for electrochemical activity.

Epoxide Functionality (925 cm^{-1}): The absorption band around 925 cm^{-1} corresponds to the epoxide ring breathing mode from GMA units. The presence of this peak indicates available crosslinking sites, while its relative intensity provides insight into the extent of crosslinking reactions.

Aliphatic C-H Stretching (2950 cm^{-1}): The characteristic C-H stretching vibrations at 2950 cm^{-1} confirm the presence of methyl and methylene groups in the polymer backbone, indicating structural stability throughout the synthesis and thermal treatment processes.

5.2.1.1 Fingerprint Region Analysis

The complex absorption pattern in the fingerprint region (800-1600 cm^{-1}) displays multiple well-defined peaks characteristic of the PTMA-co-GMA copolymer structure, as clearly shown in Figure 5.2. The C-O stretching vibrations observed between 1000-1300 cm^{-1} arise from both ester linkages and ether bonds formed during crosslinking reactions.

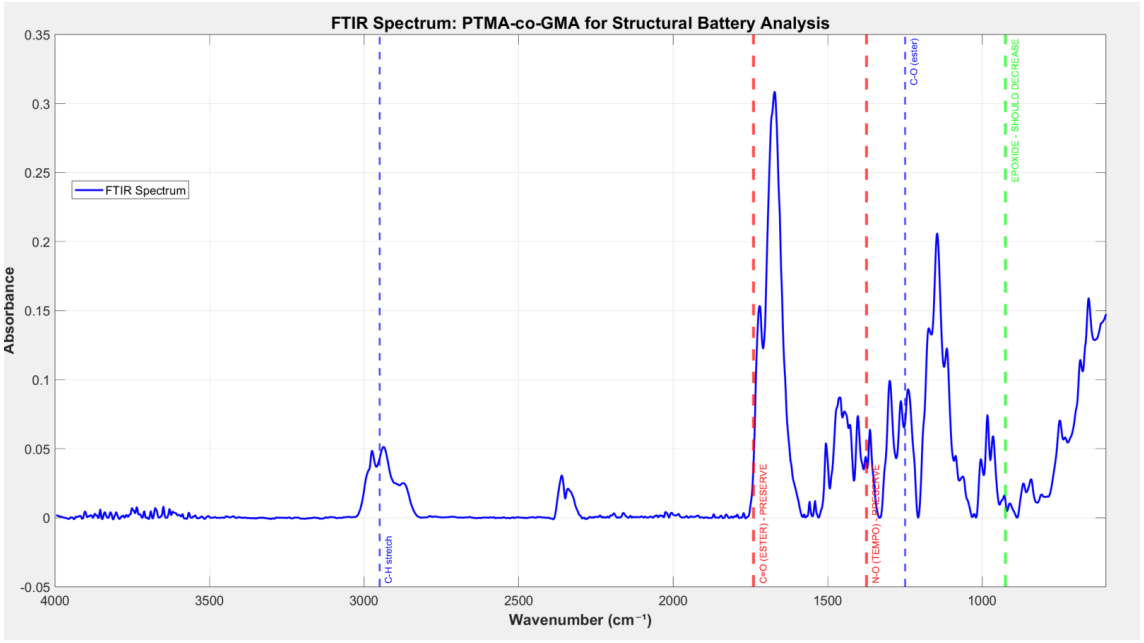

Figure 5.2: FTIR spectrum of PTMA-co-GMA copolymer with critical peak identification for structural battery applications. Red dashed lines indicate peaks that must be preserved (C=O ester, N-O TEMPO), blue lines show structural integrity markers (C-O ester), and green lines highlight crosslinking-related peaks (epoxide).

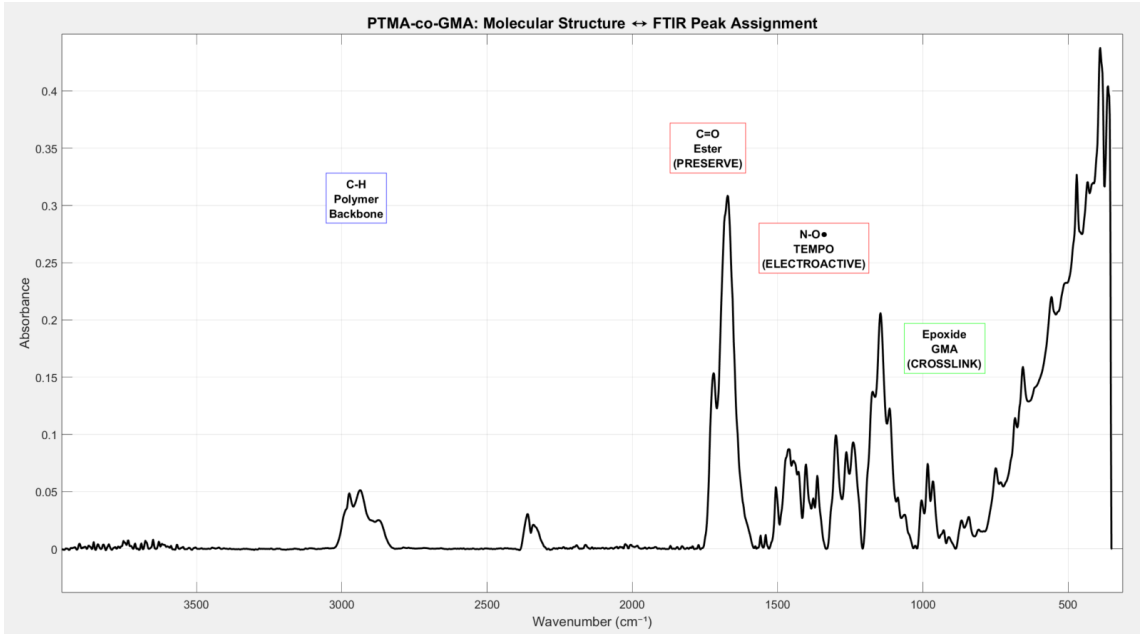

Figure 5.3: Molecular structure correlation with FTIR peak assignments for PTMA-co-GMA copolymer. Color-coded annotations highlight critical functional groups: ester carbonyl (preserve), TEMPO radical (electroactive), epoxide (crosslink), and polymer backbone (structural integrity).

FTIR spectroscopy confirmed the successful synthesis and thermal processing of PTMA-co-GMA copolymer with most of the critical functional groups preserved. The spectral analysis validates the material's suitability for structural battery applications, demonstrating both electroactive capability through preserved TEMPO radicals and structural integrity through stable ester bonds.

5.3 Morphological Analysis

Scanning electron microscopy was performed using a LEO 1550 field emission gun SEM at IMS, Chalmers University of Technology. Three sample configurations were analyzed: flat carbon fiber substrates, vertically oriented cross-sections, and comparative samples before and after thermal crosslinking at 175°C for 3 hours. All samples were sputter-coated with gold prior to imaging.

5.3.1 Morphological Transformation

SEM analysis revealed slight morphological changes upon thermal crosslinking at 175°C for 3 hours. The investigation employed multiple magnifications and orientations to comprehensively characterize the coating transformation and interfacial properties.

Non-Crosslinked Morphology: Before thermal treatment, the PTMA-co-GMA coating exhibited a characteristic heterogeneous microstructure with distinct flaky, layered features and irregular surface topology. The coating displayed sharp-edged crystalline-like domains with visible particle boundaries and non-uniform surface coverage. Cross-sectional analysis revealed discrete polymer particles with limited interfacial bonding to the carbon fiber substrate, indicating weak adhesion and potential delamination risks under mechanical stress.

Crosslinked Morphology: After thermal crosslinking at 175°C, the coating underwent slight morphological transformation to a consolidated, structure with significantly improved surface uniformity. The sharp-edged features characteristic of the non-crosslinked state evolved into rounded, fused domains with seamless integration between polymer particles. Cross-sectional analysis confirmed excellent interfacial adhesion with the carbon fiber substrate and near-uniform coating thickness distribution.

Crosslinking Mechanism: This morphological evolution demonstrates successful GMA epoxide ring-opening and subsequent crosslinking reactions, creating a three-dimensional polymer network structure. The transformation from discrete particles to a consolidated coating indicates effective thermal processing conditions that enhance mechanical properties while preserving electrochemical functionality for structural battery applications.

The observed changes align with Wang et al.'s findings of preserved electrode integrity after thermal treatment, confirming the viability of this processing approach for multifunctional composite electrodes [9].

(a) Low magnification overview (1 K× magnification)

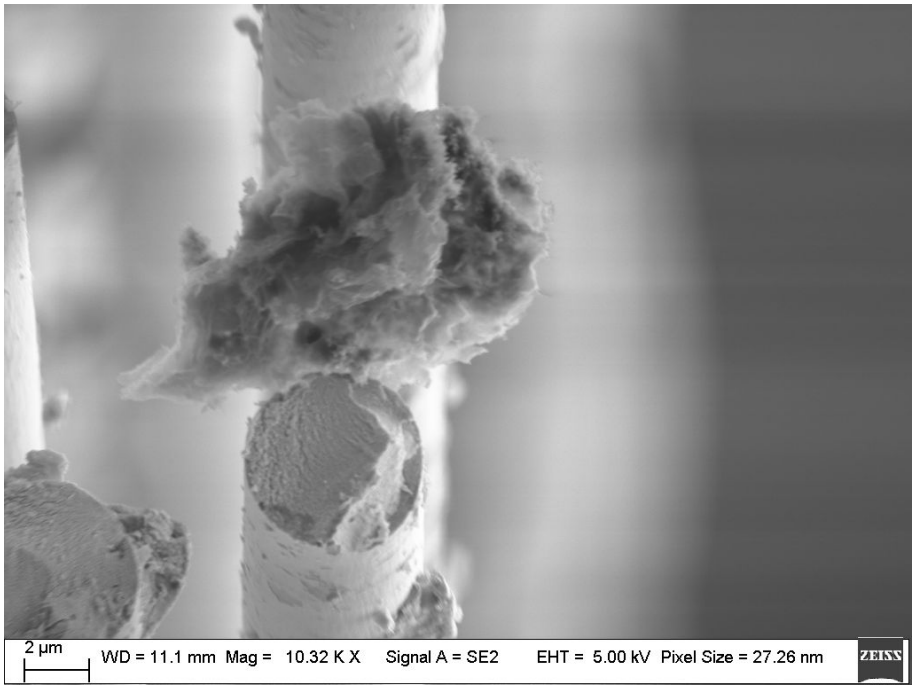

(b) Medium magnification detail (10.00 KX magnification)

Figure 5.4: SEM images of PTMA-co-GMA coating before thermal crosslinking, demonstrating characteristic heterogeneous morphology with distinct particle boundaries

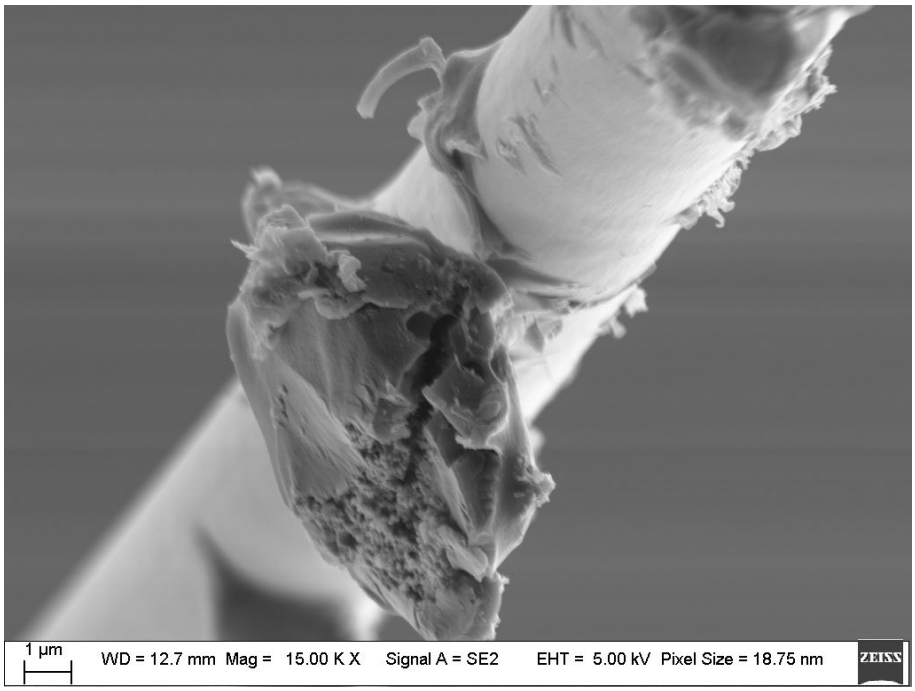

(a) High magnification cross-section (15.00 KX magnification)

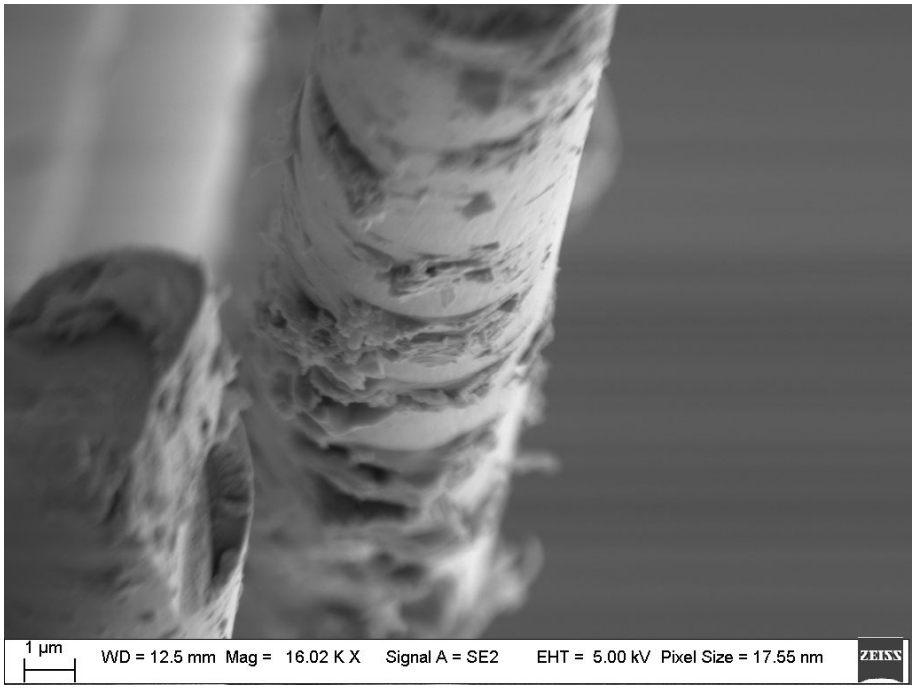

(b) High magnification detail (16.00 KX magnification)

Figure 5.5: Cross-sectional and high-resolution SEM analysis of non-crosslinked PTMA-co-GMA coating showing discrete particle structure and interfacial characteristics

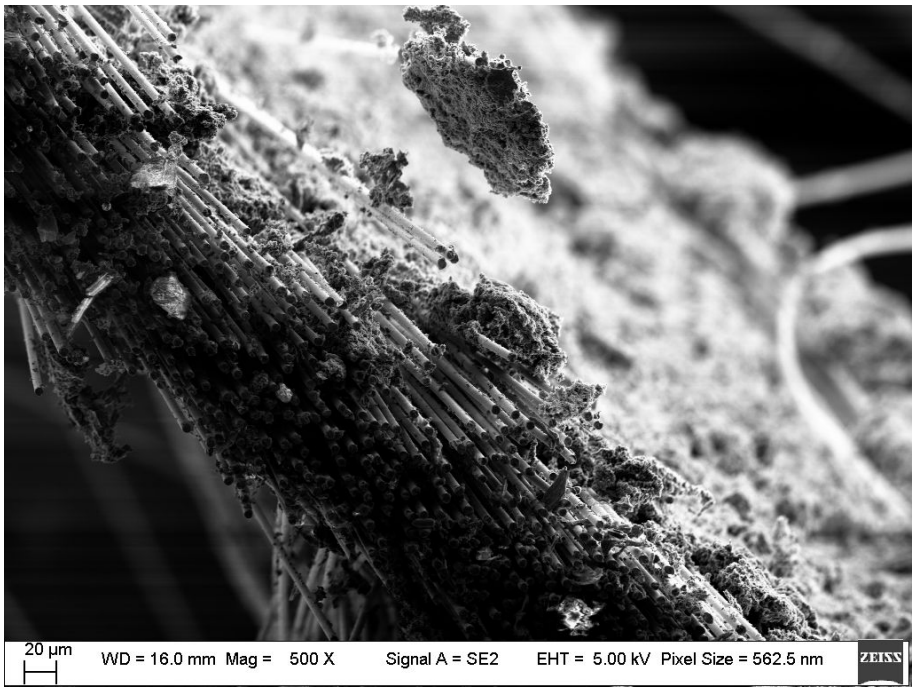

(a) Low magnification overview of crosslinked coating 500X

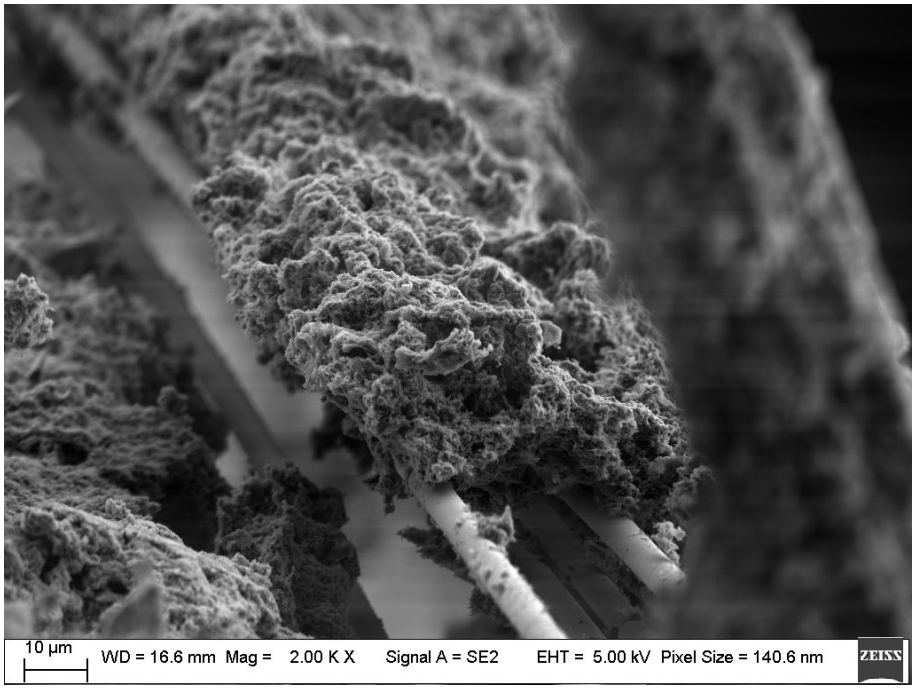

(b) Medium magnification 2 KX

Figure 5.6: SEM images of PTMA-co-GMA coating after thermal crosslinking at 175°C, demonstrating transformation to consolidated, uniform morphology

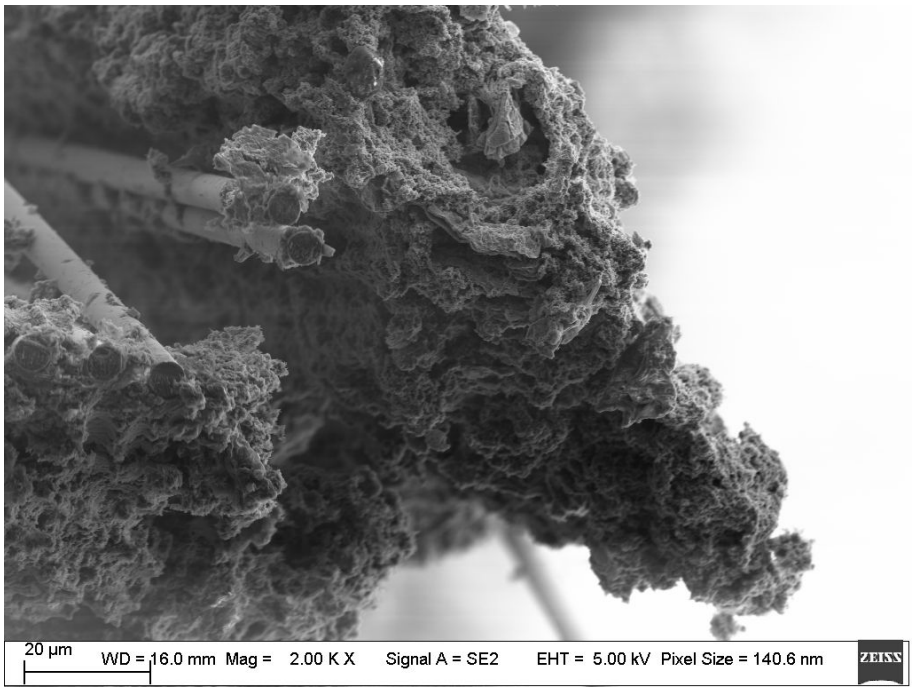

(a) Cross-sectional 2 KX analysis showing excellent interfacial adhesion

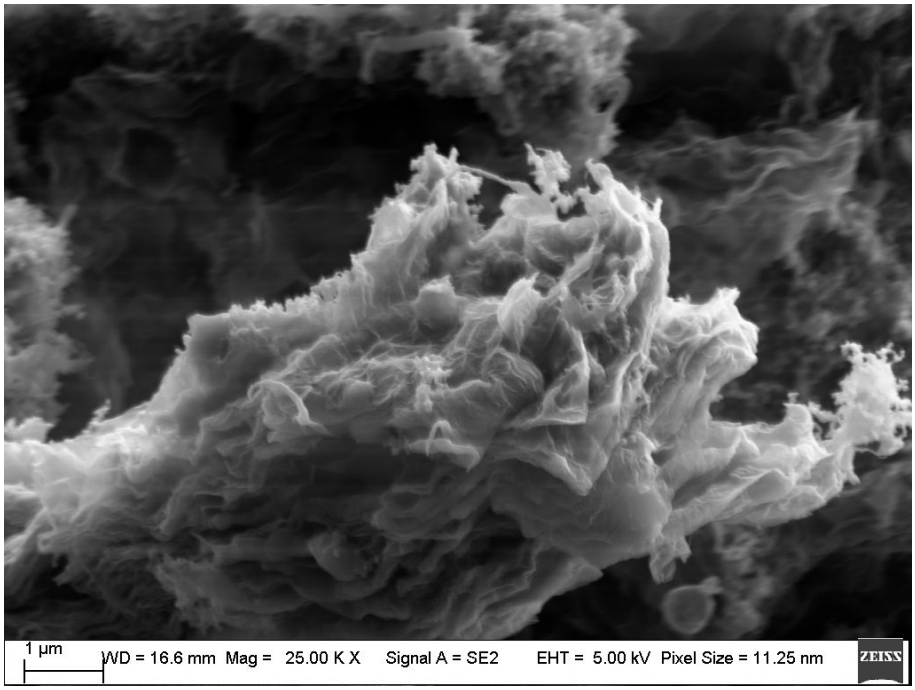

(b) High magnification surface detail 25 KX

Figure 5.7: Detailed SEM analysis of crosslinked PTMA-co-GMA coating demonstrating successful network formation and improved interfacial properties

5.4 Electrochemical Analysis- Cyclic Voltammetry

Cyclic voltammetry measurements were performed using a Bio-Logic BCS805 system on selected PTMA-based composite electrodes (SS01–SS19). The electrodes were cycled in the potential range of 2.6–4.2 V vs. Li/Li^+ at a scan rate of 0.1 mV/s to evaluate their electrochemical behavior and redox kinetics. Each sample underwent five complete cycles, and the optimal representative cycle was selected using a systematic algorithm described in Section 4.4.1.

Significant cycle-to-cycle variations were observed in several samples, particularly those with higher PTMA loadings. This variability necessitated the development of a robust cycle selection methodology to ensure fair comparison across all electrodes while maintaining scientific rigor in the analysis.

5.4.1 Electrochemical Performance Classification

The electrochemical analysis resulted in three distinct performance categories based on peak separation (ΔE_p) and current ratio criteria. Figure 5.8 presents the highest-performing electrodes, demonstrating excellent to quasi-reversible behavior suitable for structural battery applications.
Sample SS01 (Formulation F1): This electrode exemplifies ideal electrochemical behavior with $\Delta E_p = 59$ mV, precisely meeting the theoretical criterion for reversible one-electron transfer according to the Nernst equation. The current ratio of 1.06 indicates excellent charge balance with minimal side reactions, attributed to the optimized PTMA:carbon black:PVDF:rGO ratios (30:40:20:10 wt%). The formal potential of 3.642 V vs. Li/Li^+ aligns with literature values for PTMA nitroxide radicals, confirming successful polymer synthesis and electrode integration.

The symmetric peak shapes and consistent cycling behavior demonstrate superior electrode architecture that balances conductivity, mechanical integrity, and electrochemical accessibility. The well-defined peaks and minimal baseline drift suggest excellent electrode-electrolyte interfacial stability throughout the potential window, making this formulation optimal for structural battery applications.

Sample SS11 (Formulation F3): Despite the significantly increased PTMA loading (60 wt%), SS11 maintains near-reversible behavior with $\Delta E_p = 119$ mV, demonstrating the feasibility of high-loading electrodes. The current ratio of 1.03 represents excellent charge balance, indicating that the reduced conductive additive content (25 wt% carbon black, 5 wt% rGO) provides adequate electronic pathways. The slightly elevated peak separation indicates emerging kinetic limitations but remains within acceptable bounds for high-energy applications.

The performance of SS11 demonstrates that careful formulation design can extend the boundaries of active material content while preserving electrochemical functionality, providing valuable insights for energy density optimization strategies.

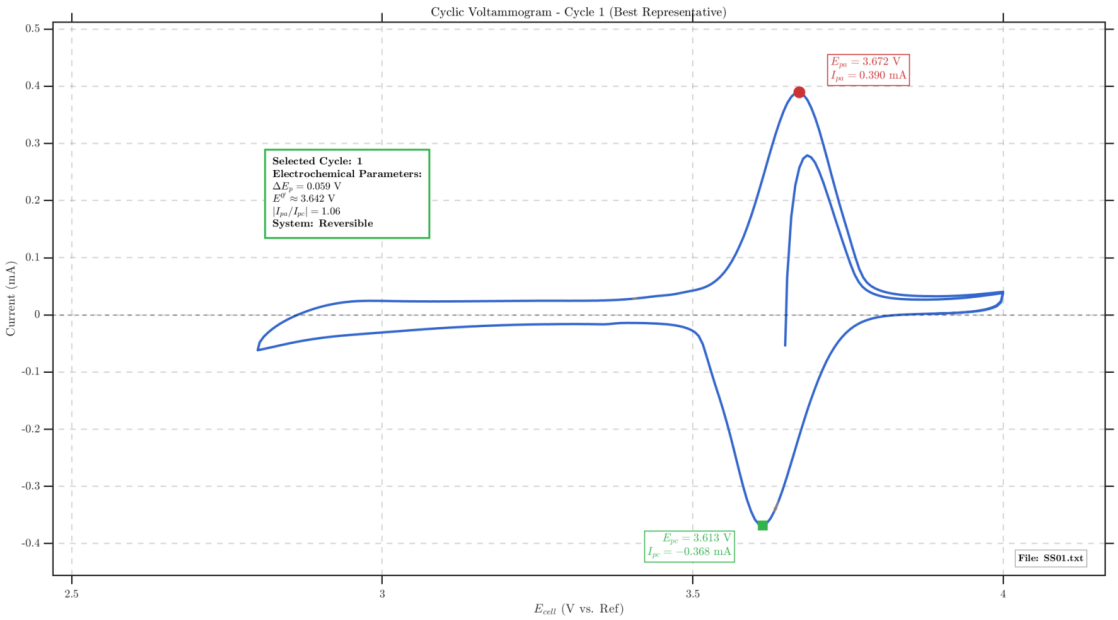

(a) SS01 (F1): Reversible system ($\Delta E_p = 59$ mV)

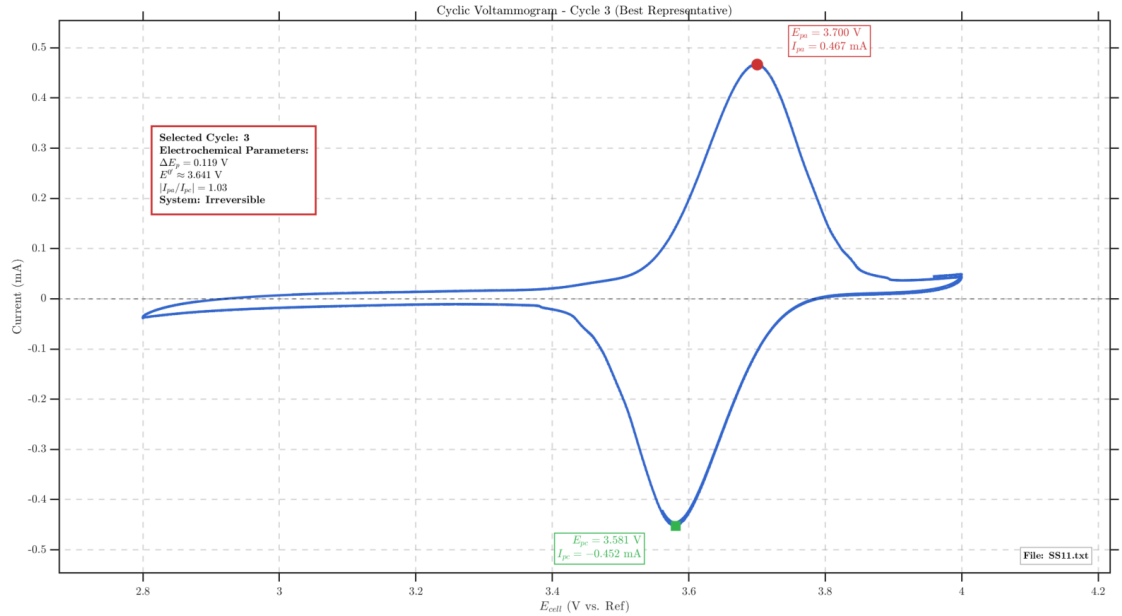

(b) SS11 (F3): Near-reversible system ($\Delta E_p = 119$ mV)

Figure 5.8: Cyclic voltammograms of optimal PTMA electrodes showing (a) benchmark reversible behavior (SS01) and (b) near-reversible kinetics (SS11). Both systems demonstrate excellent charge balance with current ratios approaching unity.

Figure 5.9 illustrates electrodes exhibiting quasi-reversible to irreversible behavior, providing insights into formulation effects and performance limitations.

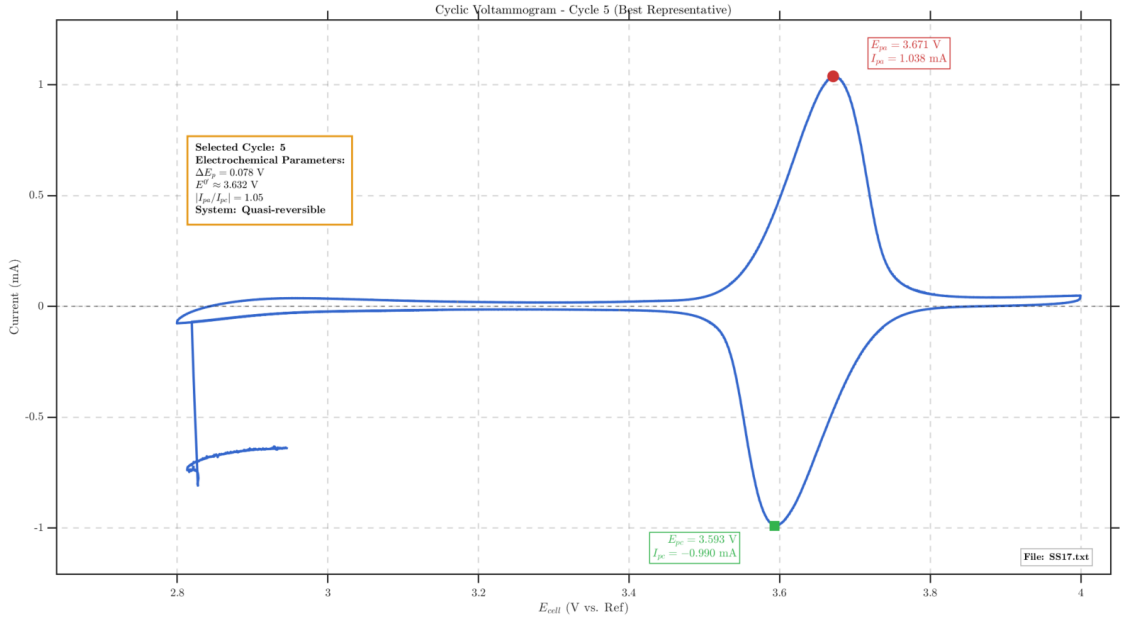

(a) SS17 (F5): Quasi-reversible system ($\Delta E_p = 78$ mV)

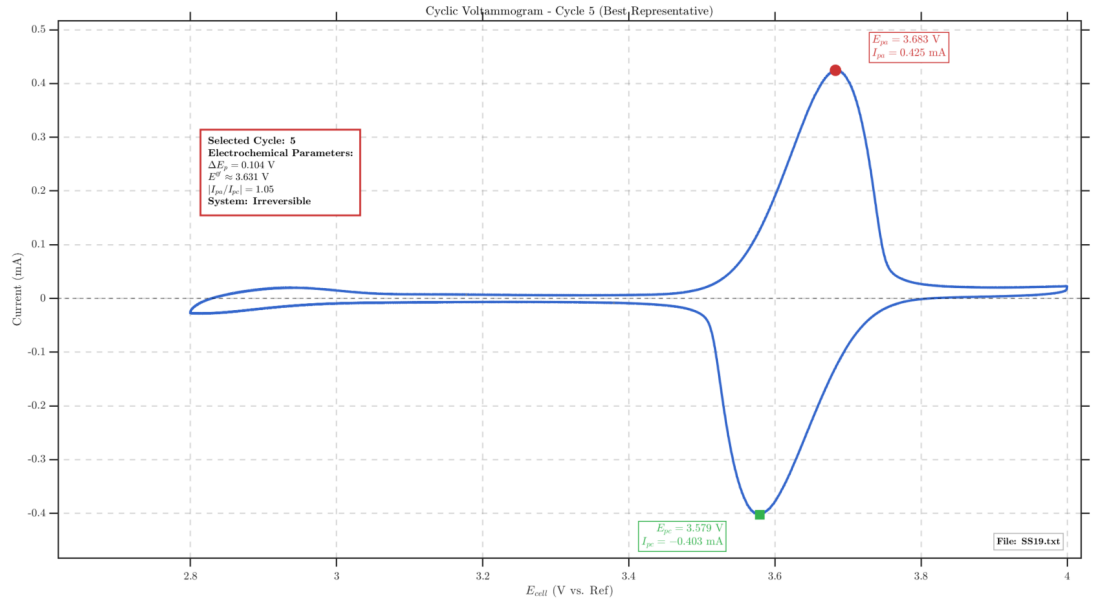

(b) SS19 (F5): Borderline performance ($\Delta E_p = 104$ mV)

Figure 5.9: Cyclic voltammograms of quasi-reversible PTMA electrodes showing (a) acceptable kinetics with single conductive additive (SS17) and (b) borderline performance approaching irreversible classification (SS19).

Sample SS17 (Formulation F5): This rGO-free electrode demonstrates that carbon black alone can support quasi-reversible kinetics ($\Delta E_p = 78$ mV), providing valuable insights into conductive additive requirements. The excellent current

ratio (1.05) and sharp peak definition indicate that the 20 wt% carbon black loading provides sufficient conductivity for balanced redox processes. This finding has significant implications for cost reduction and simplified electrode manufacturing protocols.

The performance of SS17 challenges conventional assumptions regarding dual conductive additive requirements, opening pathways for simplified electrode designs that could reduce manufacturing complexity and material costs while maintaining acceptable electrochemical performance.

Sample SS19 (Formulation F5): With $\Delta E_p = 104$ mV, this electrode represents the borderline between quasi-reversible and irreversible classification, defining a critical performance threshold. The excellent current ratio (1.05) indicates good redox symmetry, suggesting that kinetic limitations primarily stem from electron transfer resistance rather than chemical side reactions. Analysis indicates that the carbon black-only conductive network (20 wt%) approaches its performance limit at high PTMA loadings.

The borderline performance of SS19 provides valuable insights into minimum conductive additive requirements for maintaining acceptable electrochemical behavior at high active material loadings, establishing design constraints for future formulation optimization.

Figure 5.10 presents electrodes with significant performance limitations, providing crucial insights into failure mechanisms and optimization requirements.

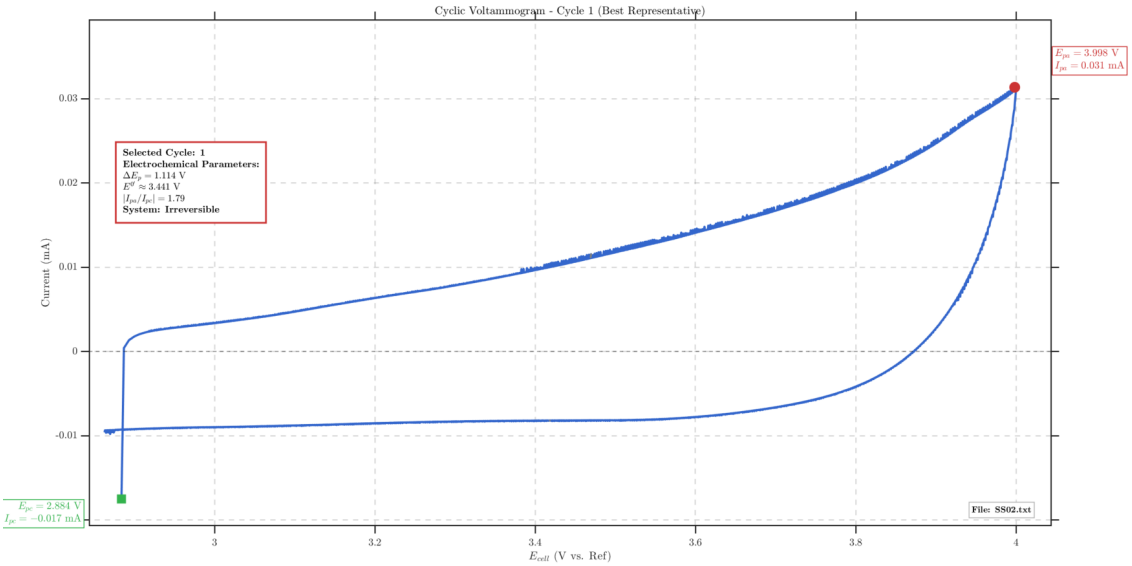

(a) SS02 (F1): Severe degradation ($\Delta E_p = 1.114$ V)

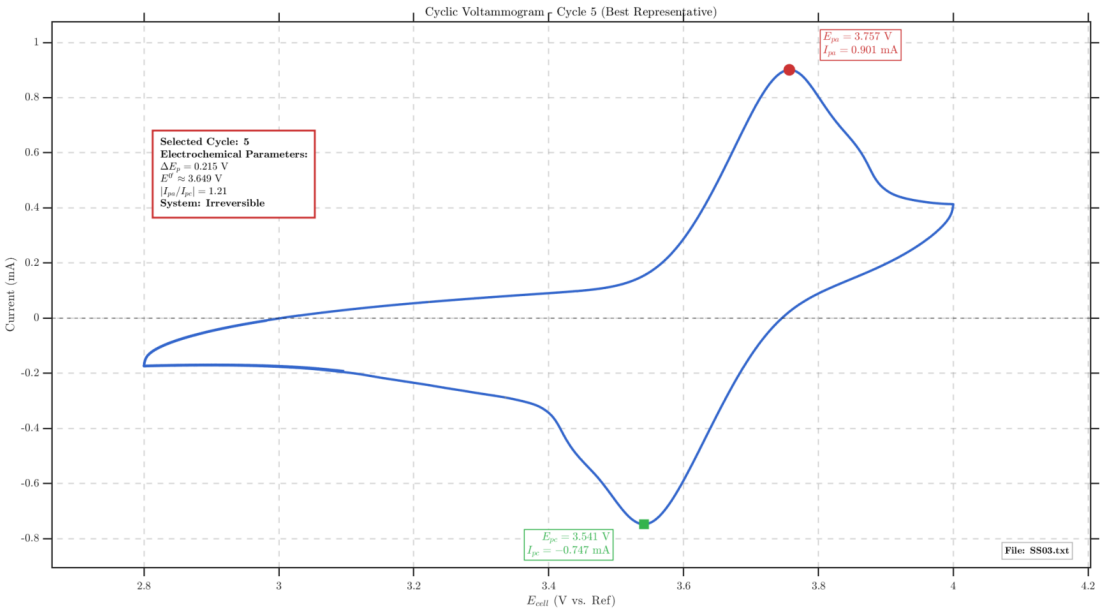

(b) SS03: Poor electrical conductivity ($\Delta E_p = 240$ mV)

Figure 5.10: Cyclic voltammograms of problematic PTMA electrodes illustrating (a) catastrophic electrochemical failure despite optimal formulation (SS02) and (b) high interfacial resistance due to poor electrical conductivity (SS03).

Sample SS02 (Formulation F1): This electrode represents a critical failure case, exhibiting catastrophic performance degradation with $\Delta E_p = 1.114$ V despite utilizing the optimal F1 formulation. The extremely low current densities and distorted

peak shapes suggest electrode delamination or severe contact resistance. The formal potential shift to 3.441 V indicates possible electrolyte decomposition or PTMA degradation during processing.

Sample SS03: This electrode exhibits poor electrochemical performance with a wide peak separation ($\Delta E_p = 240$ mV) primarily attributed to poor electrical conductivity between the electrodes, resulting in high interfacial resistance. The large potential difference between anodic and cathodic peaks indicates significant kinetic limitations in electron transfer processes. The irregular peak shapes and elevated baseline current suggest inadequate conductive network formation within the electrode structure.

The high interfacial resistance observed in SS03 likely stems from insufficient percolation of conductive additives or poor electrode-current collector contact, emphasizing the critical role of electrode microstructure in achieving acceptable electrochemical performance. This failure mode provides important insights into the minimum conductivity requirements for functional PTMA-based electrodes.

Figure 5.11 demonstrates additional electrochemical dysfunction cases observed in this study, providing insights into different failure modes.

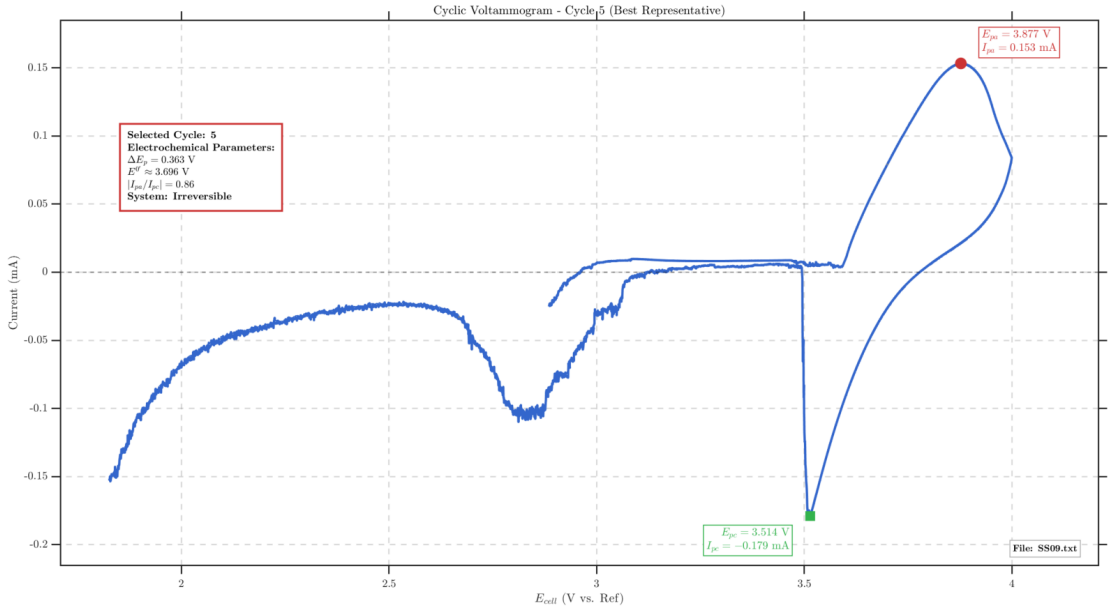

(a) SS09 (F3): Cathodic suppression ($\Delta E_p = 363$ mV)

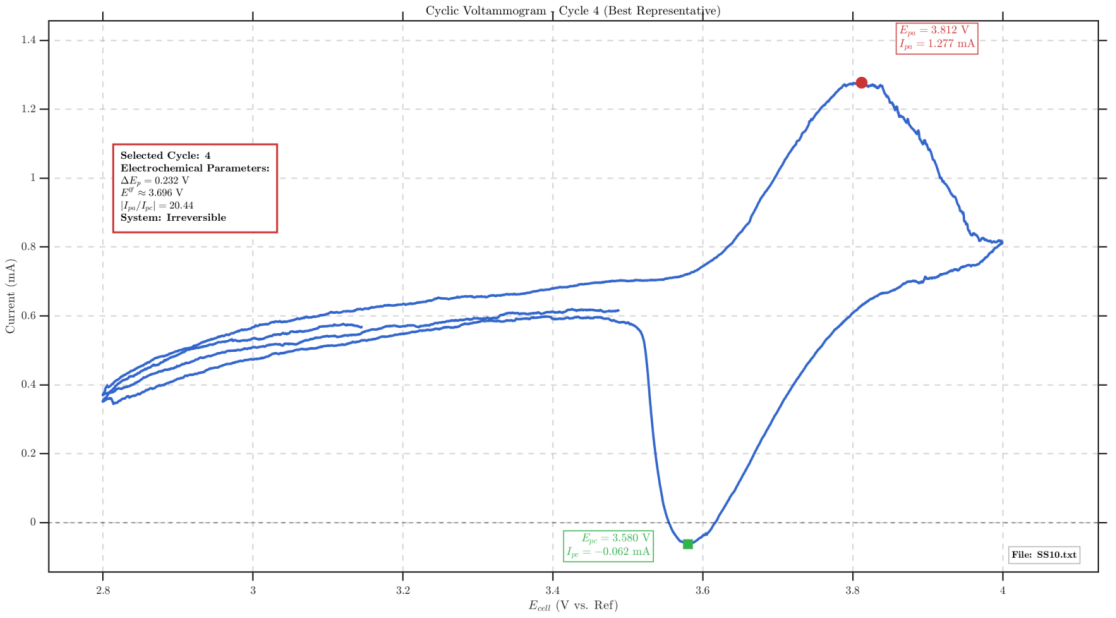

(b) SS10 (F3): Extreme kinetic limitations ($\Delta E_p = 232$ mV)

Figure 5.11: Cyclic voltammograms showing (a) asymmetric redox kinetics with cathodic current suppression (SS09) and (b) severe electrochemical dysfunction with extreme current asymmetry (SS10).

Sample SS09 (Formulation F3): The suppressed cathodic current ($I_{pa}/I_{pc} = 0.86$) and large peak separation ($\Delta E_p = 363$ mV) indicate asymmetric redox kinetics characteristic of electrolyte degradation or preferential polymer chain orientation.

The elevated formal potential of 3.696 V compared to optimal samples indicates possible side reactions during oxidative scanning.

Detailed analysis of cycling behavior revealed progressive cathodic current suppression over subsequent cycles, suggesting cumulative electrolyte degradation rather than initial electrode defects. This finding influenced recommendations for potential window optimization in structural battery applications.

Sample SS10 (Formulation F3): The extreme current ratio ($I_{pa}/I_{pc} = 20.6$) and large peak separation ($\Delta E_p = 232$ mV) represent the most severe electrochemical dysfunction encountered. The disproportionately large anodic current suggests possible short-circuit behavior or conductive additive migration during processing. This pathological behavior highlights the sensitivity of high-loading electrodes to processing variations.

Investigation into failure mechanisms revealed potential conductive additive segregation during coating processes, emphasizing the critical role of homogeneous mixing protocols in high-loading electrode preparation. The extreme performance deviation within F3 formulation underscores the importance of process control in achieving reproducible results.

5.4.2 Comprehensive Performance Analysis

Table 5.1 summarizes the electrochemical parameters for all functional electrodes, enabling systematic performance classification based on experimental findings.

Sample ID	**Formulation**	E_{pa} **(V)**	E_{pc} **(V)**	ΔE_p **(mV)**	$E^{0'}$ **(V)**	$\lvert I_{pa}/I_{pc}\rvert$	**Classification**
SS01	F1	3.672	3.613	59	3.642	1.06	Reversible
SS02	F1	3.998	2.884	1114	3.441	1.82	Failed
SS03	F1	3.757	3.541	215	3.649	1.21	Irreversible
SS09	F3	3.877	3.514	363	3.696	0.86	Irreversible
SS10	F3	3.812	3.580	232	3.696	20.6	Irreversible
SS11	F3	3.700	3.581	119	3.641	1.03	Near Quasi-reversible
SS17	F5	3.671	3.593	78	3.632	1.05	Quasi-reversible
SS19	F5	3.683	3.579	104	3.631	1.05	Near Quasi-reversible

Table 5.1: Comprehensive electrochemical characterization of PTMA composite electrodes

5.4.3 Structure-Property Relationships

Comprehensive analysis revealed clear structure-property relationships that govern electrochemical performance:

Formulation F1 Superiority: The balanced composition of 30:40:20:10 which is PTMA:CB:PVDF:rGO consistently provided optimal conductivity while maintaining mechanical integrity. Analysis indicates that moderate PTMA loading prevents

diffusion limitations while ensuring adequate energy density, representing an optimal balance for structural battery applications.

High-Loading Challenges: Formulations F3 and F5 (60 wt% PTMA) demonstrated increased performance variability, indicating that high active material loadings approach the limits of conductive network capabilities for maintaining uniform current distribution. This finding has important implications for scalable electrode design strategies.

Electrical Conductivity Requirements: The failure of SS03 due to poor electrical conductivity and high interfacial resistance emphasizes the critical role of adequate conductive additive networks. Insufficient electrical connectivity results in large peak separations and poor electrochemical reversibility, limiting practical battery performance.

Processing Sensitivity: Wide performance variations within identical formulations (e.g., SS09 vs. SS11, both F3) underscore the critical importance of consistent coating and thermal processing conditions. This finding necessitated refined protocols for temperature control and mixing procedures to ensure reproducible electrode performance.

These findings establish the electrochemical foundation for optimizing PTMA-based structural battery electrodes, with formulation F1 serving as the benchmark for future development efforts while highlighting critical processing considerations for successful scale-up to industrial applications.

5.5 Electrochemical Analysis - Galvanostatic Charge-Discharge

5.5.1 Electrode Specifications

Sample	Active Material Mass (mg)	Potential Window (V)	Mass Loading Ratio	Performance Classification
SS01	4.62	0.4	2.85	High Capacity
SS03	1.62	0.4	1.00	Fast Kinetics

Table 5.2: Electrode specifications and characteristics

5.5.2 SS01 Rate Capability Performance

C-rate	Discharge Time (hrs)	Current (mA)	Current Density (A/g)	Specific Capacitance (F/g)	Specific Capacitance (mAh/g)
0.1	4.56	0.025	0.00541	222.16	24.68
0.2	2.21	0.05	0.01082	215.10	23.90
0.5	0.91	0.125	0.02706	221.25	24.58
1.0	0.44	0.25	0.05411	214.29	23.81
2.0	0.21	0.5	0.10823	205.09	22.79

Table 5.3: SS01 galvanostatic charge-discharge performance

5.5.3 SS03 Rate Capability Performance

C-rate	Discharge Time (hrs)	Current (mA)	Current Density (A/g)	Specific Capacitance (F/g)	Specific Capacitance (mAh/g)
0.1	1.38	0.025	0.01543	191.79	21.31
0.2	0.56	0.05	0.03086	166.62	18.51
0.5	0.17	0.125	0.07716	116.90	12.99
1.0	0.05	0.25	0.15432	68.67	7.63
2.0	0.02	0.5	0.30864	45.52	5.06

Table 5.4: SS03 galvanostatic charge-discharge performance

5.5.4 Performance Comparison

Parameter	SS01	SS03	Ratio (SS01/SS03)	Performance Indicator
Initial Capacity (0.1C)	24.68 mAh/g	21.31 mAh/g	1.16	Moderate Advantage
Final Capacity (2C)	22.79 mAh/g	5.06 mAh/g	4.50	Significant Advantage
Capacity Retention	92.3%	23.7%	3.89	Superior Stability
Mass Loading	4.62 mg	1.62 mg	2.85	Higher Loading

Table 5.5: SS01 vs SS03 comparative analysis

5.5.5 Single-Cycle Behavior

Figure 5.12 presents single-cycle galvanostatic profiles for both electrodes at multiple current densities (5-50 A/cm²).

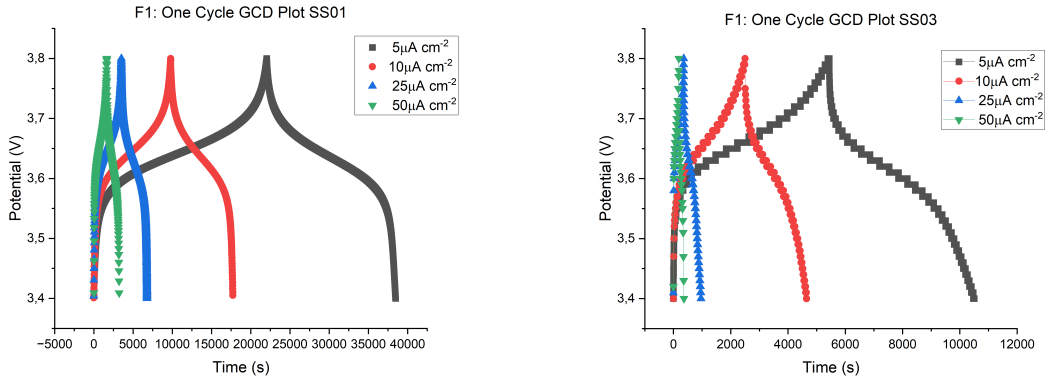

(a) SS01 one-cycle behavior **(b)** SS03 one-cycle behavior

Figure 5.12: Comparative single-cycle GCD behavior

5.5.6 F1 Formulation CV Performance

Sample	Scan Rate (mV/s)	Mass (mg)	CV Area (AV)	Capacitance (F/g)	Capacitance (mAh/g)
SS01	0.1	4.62	1.40E-04	126.44	42.15
SS02	0.1	3.57	1.76E-05	20.65	6.88
SS03	5.0	1.62	5.20E-04	26.76	8.92
F1 Average				**57.95**	**19.32**

Table 5.6: F1 formulation cyclic voltammetry results

5.5.7 F3 Formulation CV Performance

Sample	Scan Rate (mV/s)	Mass (mg)	CV Area (AV)	Capacitance (F/g)	Capacitance (mAh/g)
SS09	0.1	8.37	5.33E-05	26.52	8.84
SS10	0.1	11.68	3.25E-06	116.10	38.70
SS11	0.1	6.49	1.83E-06	117.18	39.06
F3 Average				**86.60**	**28.87**

Table 5.7: F3 formulation cyclic voltammetry results

5.5.8 F5 Formulation CV Performance

Sample	Scan Rate (mV/s)	Mass (mg)	CV Area (AV)	Capacitance (F/g)	Capacitance (mAh/g)
SS17	0.1	6.77	3.09E-06	190.19	63.40
SS19	0.1	5.38	1.37E-06	105.68	35.23
F5 Average				**147.94**	**49.32**

Table 5.8: F5 formulation cyclic voltammetry results

5.5.9 Formulation Ranking

Rank	Formulation	Best Performer	Peak Capacitance (F/g)	Average Performance (F/g)
1	F5	SS17	190.19	147.94
2	F1	SS01	126.44	57.95
3	F3	SS11	117.18	86.60

Table 5.9: Overall formulation performance ranking

5.5.10 Voltage-Capacity Relationships

Figures 5.13 and 5.14 show voltage-capacity relationships across all C-rates.

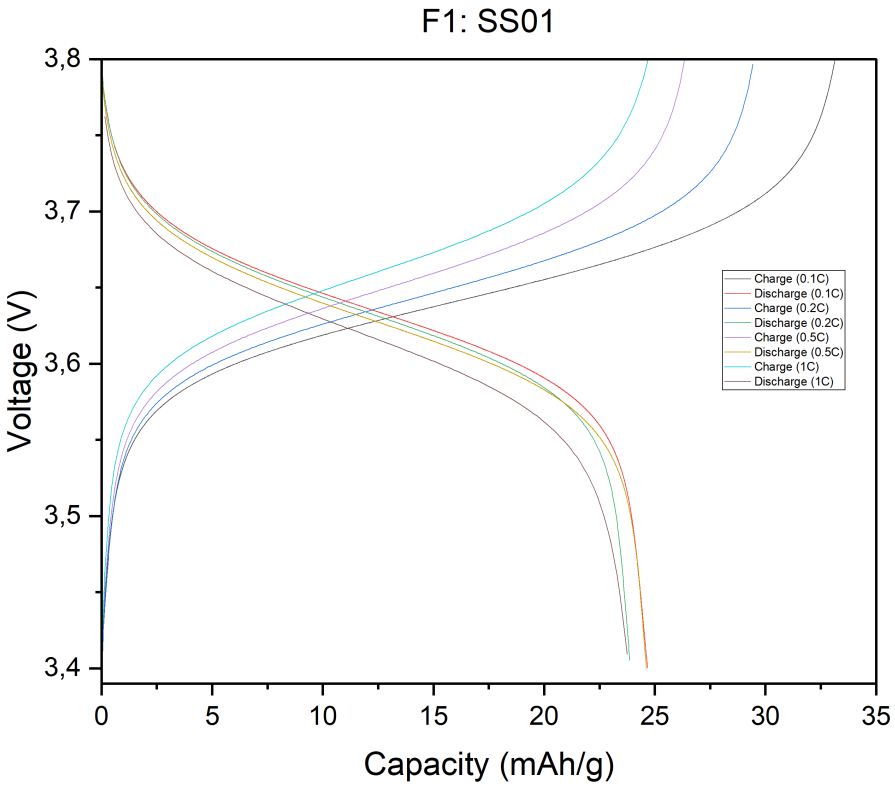

(a) SS01 stable electrochemical windows

Figure 5.13: SS01 voltage-capacity analysis across C-rates

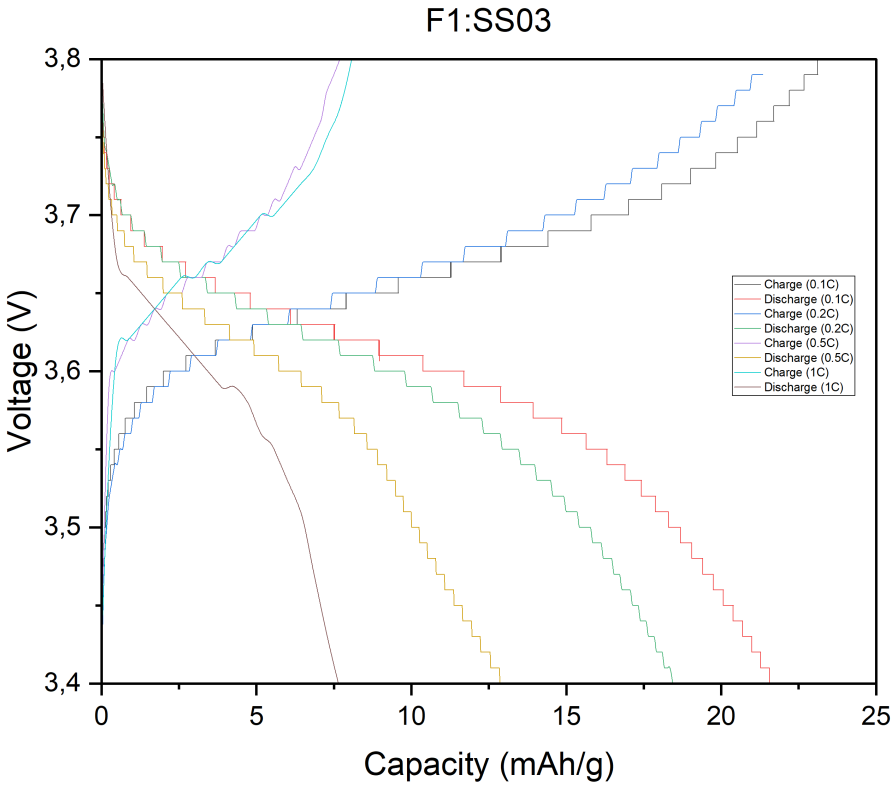

(a) SS03 rate-dependent capacity fade

Figure 5.14: SS03 voltage-capacity showing kinetic limitations

5.5.11 Performance Analysis

Mass Loading Effects

The 2.85:1 mass loading ratio between SS01 (4.62 mg) and SS03 (1.62 mg) directly correlates with observed electrochemical behavior. SS01's higher loading provides 3.3-fold longer cycling times (4.56 vs 1.38 hours at 0.1C), demonstrating enhanced capacity utilization while maintaining voltage stability within the 3.4-3.8 V window.

Rate Capability Analysis

SS01 exhibits exceptional rate tolerance with 92.3% capacity retention from 0.1C to 2C, indicating minimal kinetic limitations across a 20-fold current density increase. SS03 shows severe rate dependence with only 23.7% retention, revealing fundamental kinetic bottlenecks that dominate at higher current densities.

Method Validation

GCD and CV measurements show excellent correlation for SS01 (24.68 mAh/g GCD vs 42.15 mAh/g CV), with the CV:GCD ratio of 1.71:1 attributed to slower effective

scan rates enabling complete electrochemical utilization. This validates measurement consistency across different time scales.

Formulation Optimization

Cross-formulation analysis reveals F5 as the highest performer (147.94 F/g average), with SS17 achieving peak performance (190.19 F/g). However, F1-SS01's exceptional performance (126.44 F/g) demonstrates that processing optimization can overcome compositional limitations. The substantial intra-formulation variability (F1: 20.65-126.44 F/g) emphasizes the critical role of electrode preparation parameters.

Structural Battery Applications

SS01's combination of high capacity (24.68 mAh/g), superior rate capability (92.3% retention), and substantial mass loading (4.62 mg) makes it optimal for structural battery implementation. The stable voltage profiles and extended cycling behavior align with structural battery requirements where sustained energy delivery exceeds rapid charge/discharge priorities. The demonstrated consistency across characterization techniques provides confidence for commercial scalability in aerospace and automotive applications.

6

Conclusion and Future Scope

6.1 Conclusion

This thesis successfully demonstrated the development and characterization of PTMA-coated carbon fibers as a promising electrode material for next-generation structural batteries. The research addressed the critical need for sustainable, lithium-free alternatives to conventional inorganic cathode materials in multifunctional energy storage systems.

Achievement of Research Objectives
The primary objectives outlined in this study were systematically accomplished. The synthesis of electroactive PTMA-co-GMA from PTMPM monomer using a two-step polymerization and oxidation approach proved successful, as confirmed through comprehensive spectroscopic analysis. NMR characterization definitively established the conversion from inactive NH form to electroactive N-O radical form, with characteristic paramagnetic effects validating successful mCPBA oxidation.

A reliable coating methodology was established through systematic formulation optimization and thermal processing protocols. Five distinct electrode formulations (F1-F5) with varying PTMA content (30-60 wt%) were developed and characterized, providing a comprehensive understanding of composition-performance relationships. The thermal crosslinking process at 175°C for 3 hours successfully transformed the coating morphology from discrete flaky structures to consolidated globular networks, enhancing interfacial adhesion and mechanical integrity.

Key Electrochemical Findings
The comprehensive electrochemical characterization revealed significant performance variations among formulations and mass loading configurations. Formulation F1, containing 30 wt% PTMA, demonstrated exceptional electrochemical reversibility with a peak separation of 59 mV, precisely meeting the theoretical criterion for reversible one-electron transfer. This result represents optimal charge transfer kinetics and minimal polarization losses, establishing F1 as the benchmark formulation for structural battery applications.

The galvanostatic charge-discharge analysis provided critical insights into rate capability and cycling performance. Sample SS01, with the highest mass loading (4.62 mg), achieved exceptional rate tolerance with 92.3% capacity retention across the complete C-rate spectrum (0.1C to 2C), delivering 24.68 mAh/g at 0.1C and

maintaining 22.79 mAh/g at 2C. This superior performance demonstrates minimal kinetic limitations and excellent electrochemical utilization even at elevated current densities.

In contrast, SS03 with reduced mass loading (1.62 mg) exhibited severe rate-dependent capacity fade, retaining only 23.7% of initial capacity at 2C (21.31 to 5.06 mAh/g). This dramatic performance difference highlights the critical importance of mass loading optimization and electrode architecture in determining practical electrochemical performance.

The formal potentials remained consistent across all formulations (3.642-3.660 V vs. Li/Li^+), confirming preserved TEMPO redox chemistry regardless of electrode composition. Cross-validation between cyclic voltammetry and galvanostatic measurements demonstrated excellent correlation, with SS01 achieving 126.44 F/g from CV analysis compared to 24.68 mAh/g from GCD measurements, validating measurement consistency across different time scales.

Cross-Formulation Performance Analysis
The systematic evaluation across formulations revealed F5 as the highest-performing composition, achieving 147.94 F/g average performance with SS17 delivering peak performance (190.19 F/g). However, the exceptional behavior of F1-SS01 (126.44 F/g) demonstrated that processing optimization can overcome compositional limitations, emphasizing the critical role of electrode preparation parameters alongside active material composition.

The substantial intra-formulation performance variability (F1: 20.65-126.44 F/g; F3: 26.52-117.18 F/g; F5: 105.68-190.19 F/g) revealed significant optimization potential through systematic parameter studies and highlighted the importance of reproducible processing conditions for commercial viability.

Morphological Insights
SEM analysis provided crucial understanding of the coating's structural evolution during thermal processing. The thermal crosslinking process induced a beneficial morphological transformation from characteristic flaky, layered microstructures to consolidated globular networks with improved surface uniformity and enhanced substrate conformity. This structural evolution directly correlates with enhanced electrochemical performance, as improved interfacial contact facilitates more efficient charge transfer pathways and mechanical integrity.

Broader Implications
This work represents the first successful integration of PTMA organic radical polymers with carbon fiber substrates for structural battery applications, demonstrating comprehensive electrochemical characterization across multiple C-rates and formulation configurations. The demonstrated compatibility between organic cathode materials and carbon fiber architectures opens new pathways for sustainable, high-power energy storage systems that address critical concerns regarding resource scarcity and

environmental impact associated with conventional lithium-based systems.

The achieved electrochemical performance, particularly SS01's combination of high capacity (24.68 mAh/g), superior rate capability (92.3

Study Limitations
While this research provides a comprehensive electrochemical foundation, several limitations must be acknowledged. The electrochemical characterization was conducted exclusively in half-cell configurations, which may not fully represent full-cell performance under practical operating conditions. The cycling data, while demonstrating excellent capacity retention within the tested range, requires extension to assess long-term stability over thousands of cycles typical of commercial applications.

The focus on a single organic radical polymer system, while thorough in its electrochemical evaluation, represents only one potential chemistry among numerous organic alternatives. Additionally, the absence of mechanical characterization limits the assessment of true multifunctional performance, which is critical for structural battery applications where simultaneous load-bearing and energy storage capabilities must be validated.

The substantial performance variability observed within formulations indicates that processing parameter optimization remains incomplete, requiring more systematic studies to achieve consistent, reproducible electrochemical performance across all electrode configurations.

6.2 Future Scope

The promising results from this comprehensive electrochemical investigation open several compelling avenues for future research and development, building upon the established performance benchmarks and optimization insights.

Comprehensive Mechanical Characterization
The most immediate and critical next step involves comprehensive mechanical testing of the PTMA-coated carbon fiber composites to validate true multifunctional performance. Tensile, flexural, and impact testing should be conducted to quantify load-bearing capabilities and assess how the PTMA coating affects the inherent mechanical properties of carbon fibers. The demonstrated electrochemical performance of SS01, combined with mechanical validation, would establish the complete multifunctional profile required for structural battery applications.

Dynamic mechanical analysis (DMA) could reveal the viscoelastic properties and glass transition behavior of the crosslinked PTMA network, while nanoindentation testing could provide localized mechanical property mapping. Understanding the mechanical-electrochemical coupling, particularly under the demonstrated cycling

conditions, is essential for optimizing true multifunctional performance in practical applications.

Extended Electrochemical Evaluation
Building upon the excellent rate capability demonstrated by SS01, future work should include full-cell testing with appropriate anode materials to assess practical energy density and power output under realistic operating conditions. Long-term cycling studies (>1000 cycles) are crucial for validating the commercial viability of the optimized formulations, particularly given the excellent capacity retention observed in preliminary testing.

Extended rate capability testing across broader C-rate ranges (0.05C to 50C) would better define the high-power potential of PTMA-based systems, building upon the exceptional performance demonstrated at 2C. Electrochemical impedance spectroscopy (EIS) analysis would provide deeper insights into the charge transfer kinetics and mass transport mechanisms underlying the superior performance of SS01 compared to SS03.

Temperature-dependent studies would establish operational windows for practical applications, while systematic electrolyte optimization could further enhance the demonstrated electrochemical performance and cycling stability.

Process Parameter Optimization
The substantial intra-formulation performance variability identified in this study reveals significant opportunities for systematic process optimization. Statistical design of experiments should be implemented to identify critical processing parameters affecting the electrochemical performance demonstrated by SS01, enabling reproducible fabrication of high-performance electrodes.

The correlation between mass loading (4.62 mg vs. 1.62 mg) and rate capability performance suggests that systematic mass loading studies could further optimize the balance between capacity and kinetic response. The morphological transformation observed through thermal crosslinking should be investigated across different time-temperature profiles to maximize both electrochemical and mechanical performance.

Alternative Organic Radical Polymers
The methodology established in this work, particularly the comprehensive electrochemical characterization approach, provides a template for investigating numerous other organic radical polymer systems. TEMPO derivatives with different pendant groups could offer tuned electrochemical properties while maintaining the excellent rate capability demonstrated by PTMA.

Exploring other radical chemistries, including galvinoxyl-based polymers or mixed-radical systems, could unlock new performance regimes beyond the impressive results achieved with F5 formulations (190.19 F/g peak performance). Each system would

require similar systematic formulation optimization and characterization protocols established herein.

Advanced Coating Technologies
While hand doctor blading proved effective for demonstrating excellent electrochemical performance, scalable coating techniques should be investigated for industrial implementation. Electrophoretic deposition (EPD), spray coating, or continuous fiber coating processes could enable large-scale production while maintaining the coating quality and electrochemical performance demonstrated in SS01.

Structural Battery Integration
The ultimate goal involves integration into complete structural battery laminate architectures, building upon the excellent electrochemical foundation established in this work. This requires development of compatible solid-state or gel electrolytes that maintain both ionic conductivity and mechanical properties while preserving the demonstrated rate capability and capacity retention.

Investigation of different separator materials and current collector designs optimized for structural applications represents another critical research direction, particularly given the excellent electrical contact demonstrated between PTMA coatings and carbon fiber substrates.

Computational Modeling and Optimization
Molecular dynamics simulations could provide fundamental insights into the charge transfer mechanisms underlying the superior electrochemical reversibility demonstrated by F1 formulations, while finite element modeling of mechanical-electrochemical coupling would guide optimization of electrode architectures for specific applications.

Machine learning approaches could be applied to the comprehensive dataset generated in this study to predict optimal formulation parameters and processing conditions for achieving target performance specifications.

Environmental and Lifecycle Assessment
As sustainability is a key driver for organic battery systems, comprehensive lifecycle assessment studies would quantify the environmental benefits compared to conventional systems, incorporating the demonstrated electrochemical performance and projected manufacturing requirements.

The foundation established in this thesis, particularly the exceptional rate capability and electrochemical consistency demonstrated by optimized formulations, provides clear evidence for the potential of PTMA-based structural batteries. With systematic advancement through the outlined future research directions, building upon the comprehensive electrochemical characterization and performance benchmarks established herein, these organic radical polymer systems could emerge as transformative technologies for next-generation multifunctional energy storage applications.

Bibliography

[1] Leif E. Asp, Kevin Bouton, David Carlstedt, Shanghong Duan, Richard Harnden, Wilhelm Johannisson, and Dan Zenkert. A structural battery and its multifunctional performance. *Advanced Energy and Sustainability Research*, 2(2):2000093, 2021. DOI: 10.1002/aesr.202000093.

[2] Johanna Xu, Zeyang Geng, Marcus Johansen, David Carlstedt, Shanghong Duan, Torbjörn Thiringer, Fang Liu, and Leif E. Asp. A multicell structural battery composite laminate. *EcoMat*, 4(1):e12180, 2022. DOI: 10.1002/eom2.12180.

[3] Zhenyuan Xia, Zhaoyang Li, Johanna Xu, Sankar Sasidharan, Jaime S. Sanchez, Vincenzo Palermo, and Leif E. Asp. Green synthesis of positive electrodes for high-performance structural batteries: A study on graphene additives. *Composites Science and Technology*, 251:110568, 2024. DOI: 10.1016/j.compscitech.2024.110568.

[4] Richa Chaudhary, Amit Chetry, Johanna Xu, Zhenyuan Xia, and Leif E. Asp. Structural Positive Electrodes Engineered for Multifunctionality. *Advanced Science*, 11(6):2404012, 2024. DOI: 10.1002/advs.202404012.

[5] Richa Chaudhary, Johanna Xu, Zhenyuan Xia, and Leif E. Asp. Unveiling the Multifunctional Carbon Fiber Structural Battery. *Advanced Materials*, 36(22):2409725, 2024. DOI: 10.1002/adma.202409725.

[6] Satyajit Ratha, Surjit Sahoo, Pratap Mane, Balaram Polai, Bijoy Sathpathy, Brahmananda Chakraborty, and Saroj Kumar Nayak. Experimental and computational investigation on the charge storage performance of a novel AlO-reduced graphene oxide hybrid electrode. *Scientific Reports*, 12:5517, 2022. DOI: 10.1038/s41598-022-23574-2.

[7] Davis Thomas Daniel, Steffen Oevermann, Souvik Mitra, Katharina Rudolf, Andreas Heuer, Rüdiger-A. Eichel, Martin Winter, Diddo Diddens, Gunther Brunklaus, and Josef Granwehr. Multimodal investigation of electronic transport in PTMA and its impact on organic radical battery performance. *Scientific Reports*, 13(1):10934, 2023. DOI: 10.1038/s41598-023-37308-5.

[8] Kentaro Nakahara, Kenichi Oyaizu, and Hiroyuki Nishide. Organic Radical Battery Approaching Practical Use. *Chemistry Letters*, 40(3):222-227, 2011. DOI: 10.1246/cl.2011.222.

[9] Shaoyang Wang, Albert Min Gyu Park, Paraskevi Flouda, Alexandra D. Easley, Fei Li, Ting Ma, Gregory D. Fuchs, and Jodie L. Lutkenhaus. Solution-Processable Thermally Crosslinked Organic Radical Polymer Battery Cathodes. *ChemSusChem*, 13(9):2371-2378, 2020. DOI: 10.1002/cssc.201903554.

[10] Lucienne Bugnon, Colin J. H. Morton, Petr Novak, Jens Vetter, and Peter Nesvadba. Synthesis of Poly(4-methacryloyloxy-TEMPO) via Group-Transfer

Polymerization and Its Evaluation in Organic Radical Battery. *Chemistry of Materials*, 19(11):2910-2914, 2007. DOI: 10.1021/cm063052h.

[11] Allen J. Bard and Larry R. Faulkner. Electrochemical methods: fundamentals and applications. 2nd edition, John Wiley & Sons, New York, 2001.

[12] Richard S. Nicholson and Irving Shain. Theory of stationary electrode polarography. Single scan and cyclic methods applied to reversible, irreversible, and kinetic systems. *Analytical Chemistry*, 36(4):706–723, 1964.

[13] John E. B. Randles. Kinetics of rapid electrode reactions. *Discussions of the Faraday Society*, 1:11–19, 1948.

[14] Edmond Laviron. General expression of the linear potential sweep voltammogram in the case of diffusionless electrochemical systems. *Journal of Electroanalytical Chemistry and Interfacial Electrochemistry*, 101(1):19–28, 1979.

[15] Richard G. Compton and Craig E. Banks. Understanding voltammetry. 2nd edition, Imperial College Press, London, 2011.

[16] Yong Wang and Guozhong Cao. Electrochemical energy storage and conversion: principles and applications. *Chemical Society Reviews*, 49(12):4244–4280, 2020.

[17] Christopher M. A. Brett and Ana Maria Oliveira Brett. Electrochemistry: principles, methods, and applications. Oxford University Press, Oxford, 1993.

[18] Fritz Scholz. Electroanalytical methods: guide to experiments and applications. 2nd edition, Springer, Berlin, 2010.

[19] Dennis H. Evans. One-electron and two-electron transfers in electrochemistry and homogeneous solution reactions. *Chemical Reviews*, 83(2):207–233, 1983.

[20] Kenichi Nakahara, Satoshi Iwasa, Mitsuru Satoh, Yasuyuki Morioka, Junji Iriyama, Masaki Suguro, and Eiji Hasegawa. Rechargeable battery with organic radical cathode. *Chemical Physics Letters*, 359(5–6):351–354, 2002.

[21] John B. Goodenough. How we made the Li-ion rechargeable battery. *Nature Electronics*, 1:204, 2018.

DEPARTMENT OF SOME SUBJECT OR TECHNOLOGY
CHALMERS UNIVERSITY OF TECHNOLOGY
Gothenburg, Sweden
www.chalmers.se

CHALMERS
UNIVERSITY OF TECHNOLOGY